Geosphere

# Geochemistry and geochronology of the Jim Sage volcanic suite, southern Idaho: Implications for Snake River Plain magmatism and its role in the history of Basin and Range extension

Alexandros Konstantinou, John Valley, Ariel Strickland, Elizabeth L. Miller, Chris Fisher, Jeffrey Vervoort and Joseph Wooden

*Geosphere* 2013;9;1681-1703
doi: 10.1130/GES00948.1



**Notes**



# Geochemistry and geochronology of the Jim Sage volcanic suite, southern Idaho: Implications for Snake River Plain magmatism and its role in the history of Basin and Range extension

**Alexandros Konstantinou[1,*], John Valley[2], Ariel Strickland[2], Elizabeth L. Miller[1], Chris Fisher[3], Jeffrey Vervoort[3], and Joseph Wooden[1,4]**

[1]*Department of Geological and Environmental Sciences, Stanford University, Stanford, California 94305, USA*
[2]*Department of Geoscience, University of Wisconsin, 1215 W. Dayton Street, Madison, Wisconsin 53706, USA*
[3]*School of the Environment, Washington State University, Pullman, Washington 99164-2812, USA*
[4]*U.S. Geological Survey, Menlo Park, California 94025, USA*

## ABSTRACT

**The Jim Sage volcanic suite (JSVS) exposed in the Jim Sage and Cotterel Mountains of southern Idaho (USA) consists of two volcanic members composed of ~240 km$^3$ of Miocene rhyolite lavas separated by an interval of lacustrine sediments. It is capped by rheomorphic ignimbrite and as much as 100 m of basaltic lava flows probably derived from the central Snake River Plain (SRP) province to the north. The occurrence of volcanic vents in the JSVS links the lava flows to their local eruptive centers, while the adjacent Albion–Raft River–Grouse Creek metamorphic core complex exposes ~3000 km$^2$ of once deep-seated rocks that offer constraints on the composition of the potential crustal sources of these rhyolites. U-Pb zircon ages from the rhyolite lavas of the JSVS range from 9.5 to 8.2 Ma. The Miocene basalt of the Cotterel Mountains has an $^{87}Sr/^{86}Sr_i$ composition of 0.7066–0.7075 and $\varepsilon_{Nd(i)}$ = –3.7, and the rhyolite lavas of the JSVS have $^{87}Sr/^{86}Sr_i$ = 0.7114–0.7135 and $\varepsilon_{Nd(i)}$ values that range from –6.7 to –7.1. Zircon from the rhyolites of the JSVS range in $\delta^{18}O_{zr}$ (Vienna standard mean ocean water, VSMOW) from –0.5‰ to 5.7‰ and have $\varepsilon_{Hf(i)}$ values ranging from –0.8 to –6.8. Based on geochronology, whole-rock major elements, trace elements, isotopes (Sr and Nd), and in situ zircon O and Hf isotopic compositions, we infer that the JSVS is genetically related to the central SRP province. The eruption of the low-$\delta^{18}O$ rhyolites of the JSVS, outside of the main topographic extent of the SRP province (without the large calderas inferred for the SRP rhyolites) implies that there might be an alternative mechanism for the formation of the low-$\delta^{18}O$ signature other than the proposed assimilation of hydrothermally altered caldera blocks. One suggestion is that the north to south propagation of SRP-type low-$\delta^{18}O$ rhyolitic melt along the Albion fault led to off-axis magmatism. Another possibility is that there was prior and widespread (across a region wider than the SRP) hydrothermal alteration of the crust related to its earlier magmatic and faulting history.**

**The eruption of SRP-type lavas in the hanging wall of an evolving metamorphic core complex helps us outline the role of the SRP magmatic province in the extensional evolution of the northeastern Basin and Range. The lavas of the JSVS imply the addition of basalt, related to the SRP hotspot, to the crust beneath the Raft River Basin that provided a heat source for crustal melting and weakening of the deep crust; this led to a vertical component of crustal flow and doming during extension, after the eruption of the 9.5–8.2 Ma JSVS rhyolites. This younger than 8.2 Ma component of vertical motion during faulting of the Miocene stratified sequence of the Raft River Basin and the rotation of the Albion fault to shallower angles collectively resulted in the subhorizontal detachment structure imaged seismically beneath the Raft River Basin.**

## INTRODUCTION

Large silicic igneous complexes are commonly associated with continental flood basalt provinces (e.g., Paraná-Etendeka and North Atlantic igneous provinces; Bryan et al., 2002; Bryan, 2007), yet their origin is one of the fundamental debates in igneous petrology and geodynamics. This debate is long standing due to the complex nature of how large silicic magmatic systems are generated and magma stored for large periods of time in heterogeneous continental crust. Understanding the origin and longevity of large silicic complexes is of great importance because this magmatic activity is often associated with mineral deposits and because silicic caldera-forming supereruptions pose major safety and economic risks to society.

In the western United States, the Snake River Plain–Yellowstone (SRP-Yellowstone) volcanic province is a prominent feature, defined by low-relief topography extending ~750 km from northwestern Nevada to Yellowstone National Park (Wyoming, Montana, and Idaho; Fig. 1 inset; e.g., Pierce and Morgan, 1992, 2009; Coble and Mahood, 2012). It is one of the most productive young silicic igneous provinces on Earth, active from ca. 16.5 Ma to the present day, generating large volumes (tens of thousands of cubic kilometers) of mostly basaltic and rhyolitic magmas (e.g., Christiansen, 2001). Petrologic investigations of silicic, intensely welded outflow ignimbrites (e.g., Branney et al., 2008) surrounding the SRP have demonstrated that the SRP-Yellowstone province is capable of producing large volumes of rhyolitic ignimbrite (>1000 km$^3$) that can travel over great distances (e.g., Andrews and Branney, 2011; Ellis et al., 2011). Individual silicic eruptive centers in the central portion of the SRP are largely inferred because they are mostly buried beneath younger basalt flows, making them inaccessible for direct study. Ongoing borehole drilling studies within the SRP are trying to address some of these problems by sampling the volcanic section directly (e.g., Shervais et al.,

*Email: akonstan@alumni.stanford.edu.

*Geosphere*; December 2013; v. 9; no. 6; p. 1681–1703; doi:10.1130/GES00948.1; 14 figures; 2 tables; 6 supplemental tables.
Received 15 May 2013 ♦ Revision received 6 September 2013 ♦ Accepted 4 October 2013 ♦ Published online 13 November 2013

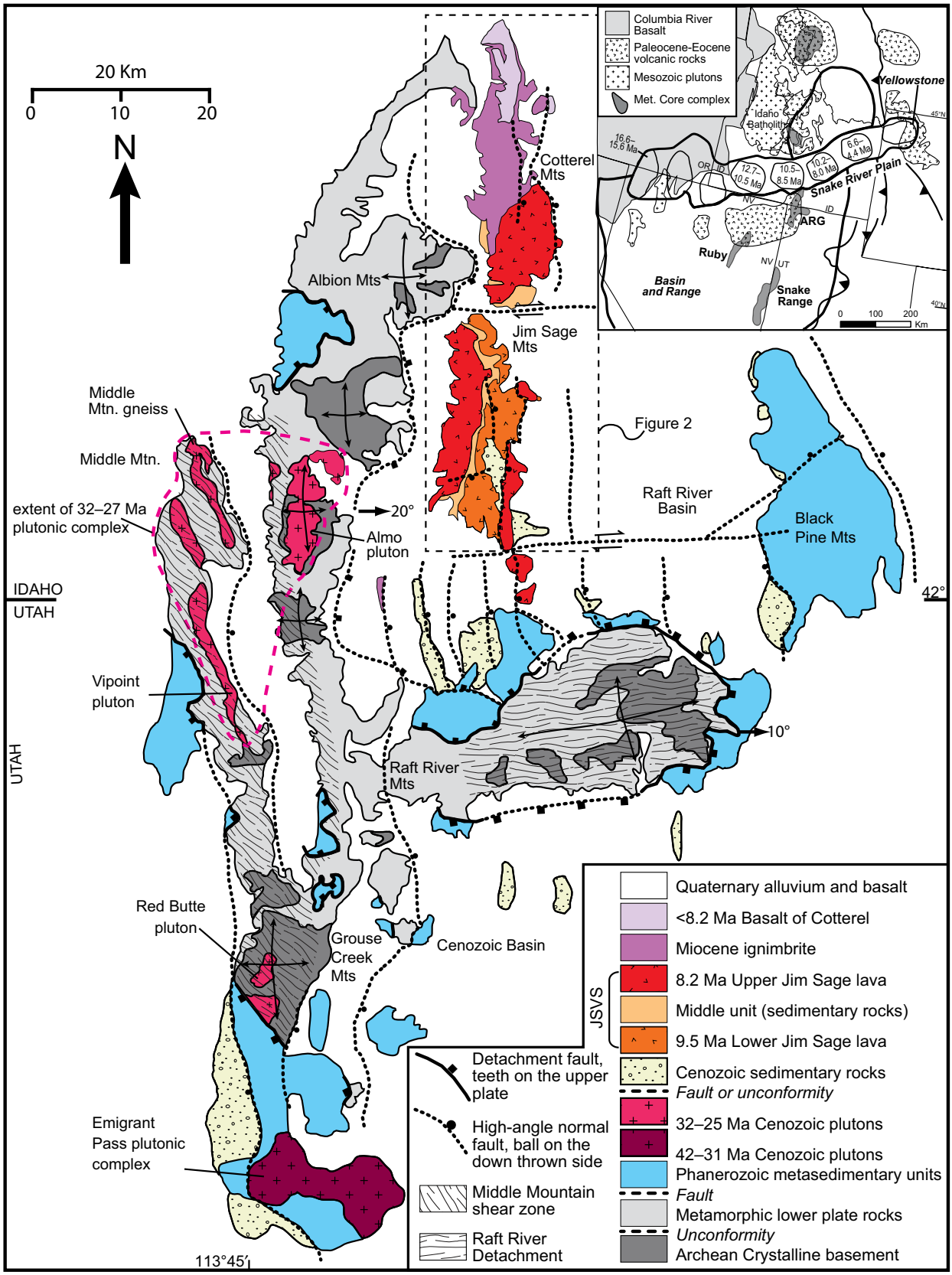


**Figure 1. Generalized geologic map of the Albion–Raft River–Grouse Creek Mountains. Box (dashed lines) indicates the location of Figure 2. Inset indicates the location of the Albion–Raft River–Grouse Creek metamorphic core complex (ARG) in the western U.S. and relative to the inferred eruptive centers in the Snake River Plain. Modified from Konstantinou et al. (2012) and references therein.**

2006; Project HOTSPOT, http://www.usu.edu/geo/shervais/Shervais-USU-Geology/Project_Hotspot.html).

Fewer studies have focused on the smaller (<300 km$^3$) eruptive centers adjacent to the SRP province that are not associated with caldera-forming eruptions but are more accessible to study. One of the best examples of such an eruptive center is the Jim Sage volcanic suite (JSVS; Fig. 1), developed within the evolving Miocene Raft River Basin (Konstantinou et al., 2012). Volcanic vents in the JSVS link the lava flows to their eruptive centers, and the adjacent Albion–Raft River–Grouse Creek metamorphic core complex exposes ~3000 km$^2$ of once deep-seated rocks that offer constraints on the composition of the basement upon which the central SRP was built. This study focuses on the petrogenesis of the volcanic rocks of the JSVS using zircon U-Pb geochronology, whole-rock major element, trace element, and isotopic compositions (Sr and Nd), and in situ zircon O and Hf isotopic compositions.

## REGIONAL GEOLOGIC SETTING

### Cenozoic Extensional and Magmatic History of the Basin and Range Province

Following the end of regional folding and thrust faulting during the Sevier and Laramide orogenies in the Cretaceous through early Cenozoic (e.g., Burchfiel et al., 1992; DeCelles et al., 1995), Paleocene–Oligocene volcanic rocks erupted across the western U.S., forming a regional pattern of magmatism that becomes younger in a southward direction across the northern Basin and Range (e.g., Christiansen and Lipman, 1972; Stewart et al., 1977; Best and Christiansen, 1991; Christiansen and Yeats, 1992; Fig. 1). Miocene extension in the Basin and Range province has been documented by crosscutting relations, the stratigraphy and age of synextensional basin fill deposits, and low-temperature thermochronology of fault blocks. These data indicate that faulting began after ca. 21 Ma and accelerated at 17–16 Ma in the central part of the northern Basin and Range (Miller et al., 1999; Stockli, 1999; Colgan et al., 2006a, 2006b, 2010; Colgan and Henry, 2009). Extensional faulting is younger at the edges of the province; rapid slip on faults began ca. 15–10 Ma in northwestern Utah and southernmost Idaho (Wells et al., 2000; Egger et al., 2003; Konstantinou et al., 2012) and in northwestern Nevada (Colgan et al., 2006b, 2008; Egger et al., 2010).

While magmatism in the Miocene SRP-Yellowstone province is largely synchronous with Miocene to present-day extension in the Basin and Range province, few studies have tried to explain how Basin and Range extension is accommodated in and across the SRP-Yellowstone province (e.g., Rodgers et al., 1990, 2002; Anders and Sleep, 1992; Parsons et al., 1998; Fig. 1). In addition, there have been very few studies focused on the relation of magmatic addition from the SRP-Yellowstone province to the deep and shallow part of the crust in the region of the Basin and Range province and/or its effects on the extensional evolution of the Basin and Range (e.g., Rodgers and McCurry, 2009). The ~240 km$^3$ rhyolitic deposits of the JSVS are intercalated with deposits of the Raft River Basin, which formed due to normal faulting associated with the Miocene exhumation of the Albion–Raft River–Grouse Creek metamorphic core complex (Konstantinou et al., 2012). Thus, the JSVS provides both timing constraints and insight as to the possible genetic relationships between magmatism and extensional faulting in the Basin and Range province.

### Magmatism in the Snake River Plain

The SRP-Yellowstone is a bimodal province characterized by tholeiitic basalts and hot and dry rhyolitic magmas (e.g., Branney et al., 2008; Christiansen and McCurry, 2008; Fig. 1 inset) that have isotopic compositions that require a significant mantle component (e.g., Hildreth et al., 1991; Nash et al., 2006; McCurry and Rodgers, 2009). The province exhibits an early phase of silicic magmatism that marks a northeast time-transgressive trend from northwest Nevada to Yellowstone, inferred to reflect the passage of the North American plate over a stationary hotspot (see discussions in Morgan et al., 1984; Hooper et al., 2007; Graham et al., 2009). Initial silicic magmatism in the well-exposed High Rock caldera complex, the McDermitt complex, and other dispersed eruptive centers coincided with the early phases of Columbia flood basalt volcanism ca. 16.5 Ma (Coble and Mahood, 2012).

One of the hallmarks of the SRP-Yellowstone province is the abundance of low-$\delta^{18}$O rhyolite magmas, first noted in Yellowstone by Friedman et al. (1974). An estimated >10,000 km$^3$ of low-$\delta^{18}$O rhyolites erupted from the SRP-Yellowstone in the past 15 m.y. (e.g., Hildreth et al., 1984; Bindeman and Valley, 2001; Boroughs et al., 2005; Bindeman et al., 2007; Cathey et al., 2007, 2011). The most widely supported explanation for low-$\delta^{18}$O rhyolites [$\delta^{18}O_{wr}$ (whole rock) ~1‰–4‰] requires a significant component of oxygen to be ultimately derived from negative $\delta^{18}$O meteoric water (–10‰ to –18‰), and therefore requires assimilation (e.g., Taylor, 1986) or remelting (e.g., Bindeman and Valley, 2001) of low-$\delta^{18}$O (2‰ to <–3‰) hydrothermally altered rock. The occurrence of low-$\delta^{18}$O rhyolite in Yellowstone has been explained by the remelting of older collapsed hydrothermally altered caldera blocks (e.g., Taylor, 1986, Bindeman and Valley, 2001). This model was then adopted for the central SRP, where large-scale remelting of buried caldera blocks resulted in the formation of low-$\delta^{18}$O rhyolites (e.g., Bindeman et al., 2007; Watts et al., 2011). In the central SRP, the model implies that the hydrothermal alteration of the upper crust was synchronous with SRP magmatism and was localized above the large magma chambers within the topographic expression of the province. It also predicts that the ignimbrites and early postcaldera lavas associated with the first collapse should show no effect, and there may be a decrease in the $\delta^{18}$O signature of the ignimbrites following multiple cycles of caldera collapse; as reported from the Heise eruptive center of the central SRP (Watts et al., 2011). Later studies from the Picabo eruptive center suggested that that hydrothermal preconditioning during Basin and Range extension, followed by caldera collapse, may have resulted in the generation of overabundant low-$\delta^{18}$O rhyolites (e.g., Drew et al., 2013). An alternative view suggests that the low-$\delta^{18}$O rhyolites in the central SRP-Yellowstone rhyolites (Owyhee-Humboldt, Bruneau-Jarbidge, Twin Falls, and Picabo eruptive centers; Pierce and Morgan, 1992) were produced by melting of crustal rocks that underwent hydrothermal alteration before SRP-Yellowstone magmatism (e.g., Boroughs et al., 2005; Leeman et al., 2008), such as altered Idaho batholith rocks (Criss and Taylor 1983; Criss et al., 1984). This view implies that the low-$\delta^{18}$O magmas reflect a signature of the crustal source that underwent hydrothermal alteration before the Miocene, and thus the alteration may not be limited to just the SRP caldera complexes.

Our study of the JSVS (Figs. 2 and 3) offers insights to the origin of the low-$\delta^{18}$O rhyolites as it represents an eruptive center outside the topographic expression of the SRP province and one that is directly linked to its volcanic vents. In particular, determining the O isotope composition of the rhyolite lavas of the JSVS helps to constrain the possible age and origin of upper crustal hydrothermal alteration. In addition, the adjacent Albion–Raft River–Grouse Creek metamorphic core complex exposes ~3000 km$^2$ of once deep-seated rocks that may have had similarities in terms of age and composition to the premagmatic crust that underlies the SRP province (Fig. 1). The O-Hf isotope composition of zircon and

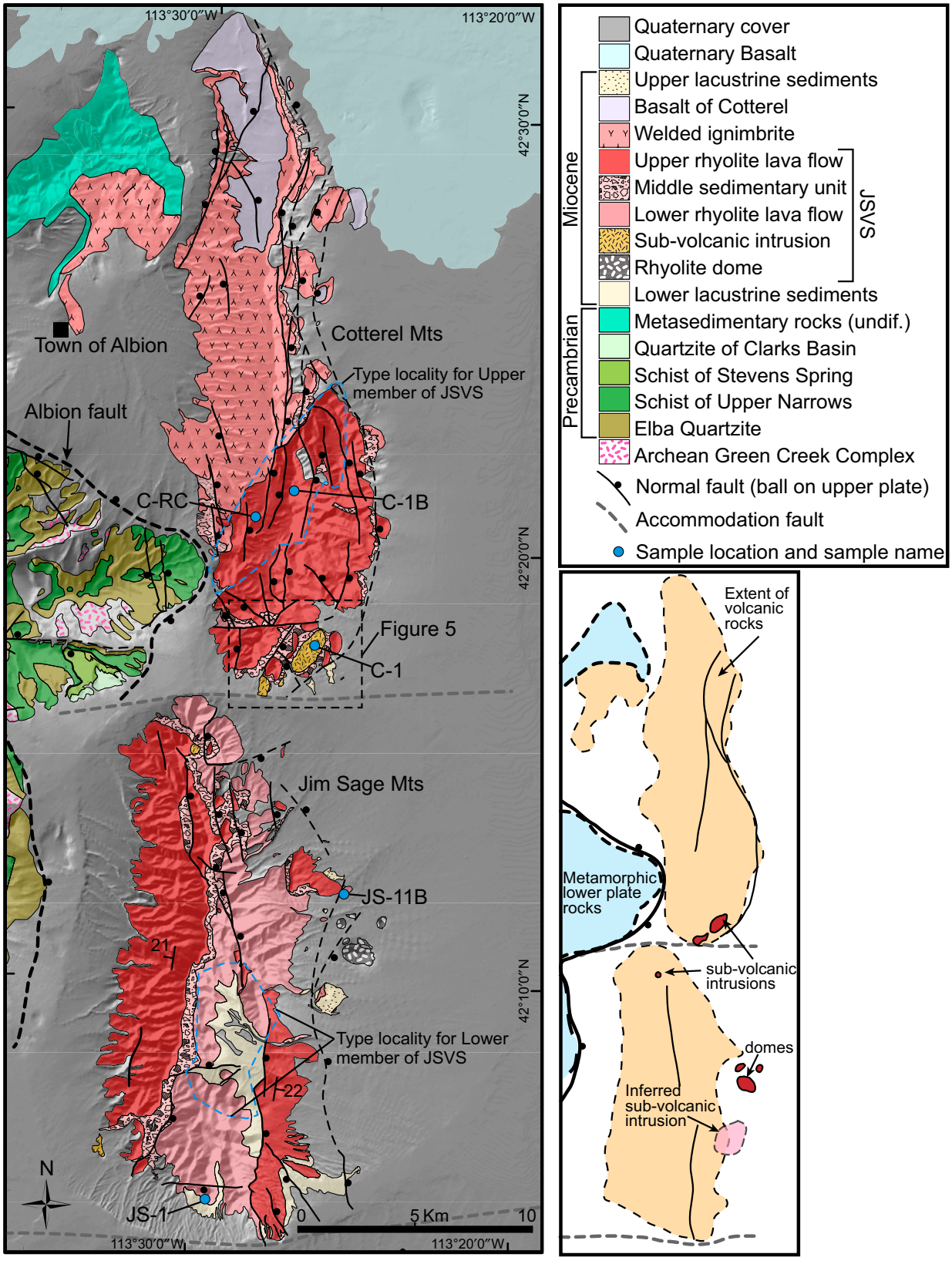


**Figure 2. Simplified geologic map of the Jim Sage volcanic suite (JSVS) and its location with respect to the Albion normal fault. Box (dashed lines) indicates the location of Figure 5. Blue dashed lines indicate the type localities for upper and lower members of the JSVS. On right is a simplified depiction with the locations of subvolcanic intrusions and domes within the Raft River Basin. Modified from existing maps by Williams et al. (1974), Smith (1982), and Pierce et al. (1983) and new geologic mapping.**

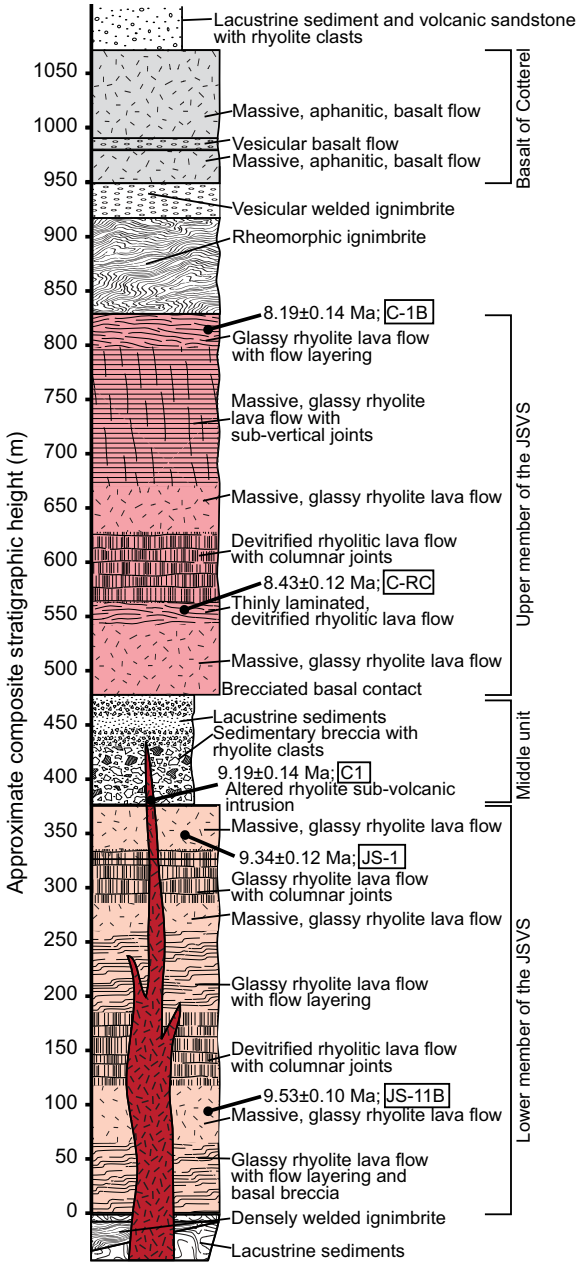


**Figure 3. Composite stratigraphy of the Jim Sage volcanic suite (JSVS) showing the stratigraphic locations of geochronology samples.**

Sr-Nd whole-rock isotopic compositions from proximal igneous and metamorphic basement rocks exposed in the metamorphic core complex have been well studied (Fig. 1; Strickland et al., 2011b; Konstantinou et al., 2013). Recent hydrogen isotope studies of ductilely deformed rocks in the Raft River Mountains show evidence for rock-meteoric fluid interaction near and along what was once the brittle-ductile transition zone in the crust. These have been interpreted to indicate circulation of meteoric water synchronous with extensional deformation and coeval with development of the mylonites within the metamorphic core complex (Gottardi et al., 2011).

## METHODS

### Geologic Mapping and Data Compilation

The JSVS crops out in the Jim Sage and Cotterel Mountains on the eastern side of the Albion Mountains, which form the northern extent of the Albion–Raft River–Grouse Creek metamorphic core complex (Figs. 1 and 2). The JSVS overlies lacustrine sedimentary rocks and is composed of two members of rhyolitic lavas separated by a sedimentary interval (Figs. 2 and 3). It is capped by ignimbrites and basaltic flows (basalt of Cotterel Mountains [Williams et al., 1982]; Fig. 2) that likely represent outflows from the central SRP. Volcanic rocks of the JSVS and associated sedimentary rocks were mapped and described as part of the Salt Lake Formation by Compton (1972, 1975), Williams et al. (1982), Covington (1983), Pierce et al. (1983), Wells (2009), and us (Konstantinou et al., 2012). Borehole, well log, and geophysical (seismic reflection, gravity, and magnetic) data initially collected for the Raft River geothermal project during the early to mid-1970s (Mabey and Wilson, 1973; Williams et al., 1974, 1982; Covington, 1983) are available for the greater Raft River Basin area, and were compiled for the purpose of this study (Konstantinou et al., 2012; Konstantinou, 2013). The Miocene Salt Lake Formation (and the JSVS) accumulated in a topographic depression or major half-graben system that formed as a response to slip along the Albion normal fault system, which bounds the basin to the west (Figs. 1 and 2) (Konstantinou et al., 2012). The onset of extensional fault slip is recorded by the age of ash-fall tuffs deposited near the base of the Miocene section ca. 14 Ma prior to the eruptions of the JSVS rhyolites (Konstantinou et al., 2012; Konstantinou, 2013; Fig. 2; part of lower lacustrine sediments).

Geologic mapping and stratigraphic investigations of the Jim Sage and Cotterel Mountains were carried out between 2009 and 2012, with attention to the basal contacts of the rhyolite flows (Figs. 2–5). These data were used to modify existing maps by Williams et al. (1974) and Pierce et al. (1983) to produce the map in Figure 2 and to better define the stratigraphy of the JSVS (Fig. 3).

### In Situ Zircon Sensitive High-Resolution Ion-Microprobe–Reverse Geometry U-Pb Geochronology

In situ zircon U-Pb analyses (n = 137) from five samples from the JSVS were carried out using the sensitive high-resolution ion-microprobe–reverse geometry (SHRIMP-RG) at the Stanford-U.S. Geological Survey Micro Analysis Center (SUMAC). Two samples were collected from the lower member of the JSVS (samples JS11-B, JS1), two samples from the upper member (samples C-RC and C1B), and one from a subvolcanic intrusion (sample C1; Table 1; Figs. 2 and 3; Supplemental Table 1[1]). Zircon was separated by crushing and various separation methods (Gemini table, heavy liquids,

[1]Supplemental Table 1. Data used to calculate zircon U-Pb ages of Miocene volcanic rocks. Geochronologic analyses performed using the SHRIMP-RG. If you are viewing the PDF of this paper or reading it offline, please visit http://dx.doi.org/10.1130/GES00948.S1 or the full-text article on www.gsapubs.org to view Supplemental Table 1.

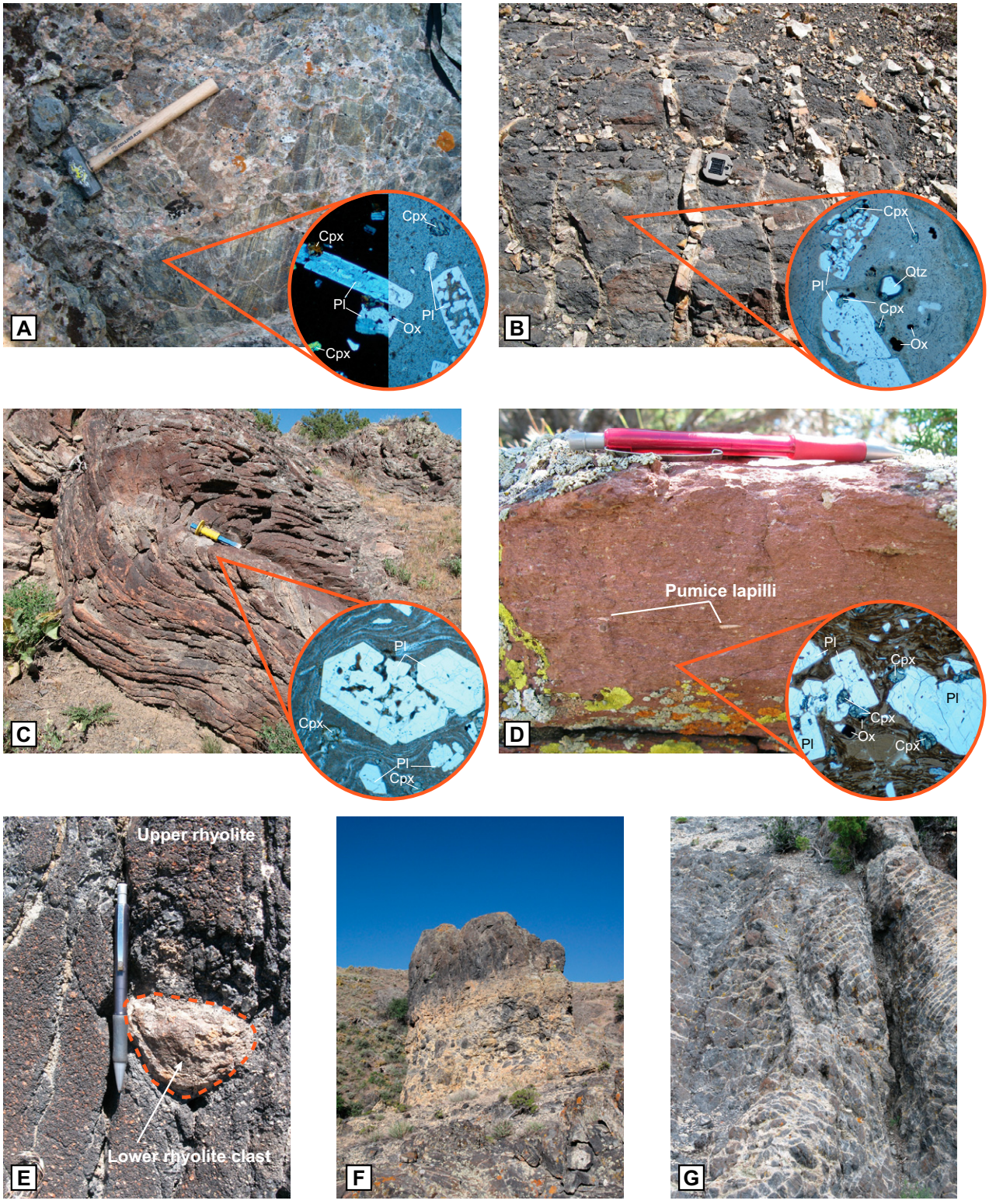


**Figure 4. Photographs and photomicrographs documenting the field relationships and thin section appearance of the rhyolite lava flows of the Jim Sage volcanic suite (JSVS) and the capping ignimbrite. Width of view of photomicrographs is 5 mm. Cpx—clinopyroxene; Ox—oxide; Pl—plagioclase; Qtz—quartz. (A) Autobrecciated base of the lower member of the JSVS. (B) Autobrecciated base of upper member of the JSVS. (C) Rheomorphic ignimbrite of the upper member of the JSVS. Note the transposed and deformed shards in the photomicrograph. (D) Distal facies of the welded ignimbrite capping the upper member of the JSVS, highlighting collapsed pumice lapilli and the deformed glass shards in the photomicrograph. (E) Basal lava flow of the upper member of the JSVS with an entrained clast of the lower member. (F) Basal autobreccia of the lower member of the JSVS. (G) Autobreccia at the top of the lower member (base of the middle unit) of the JSVS.**

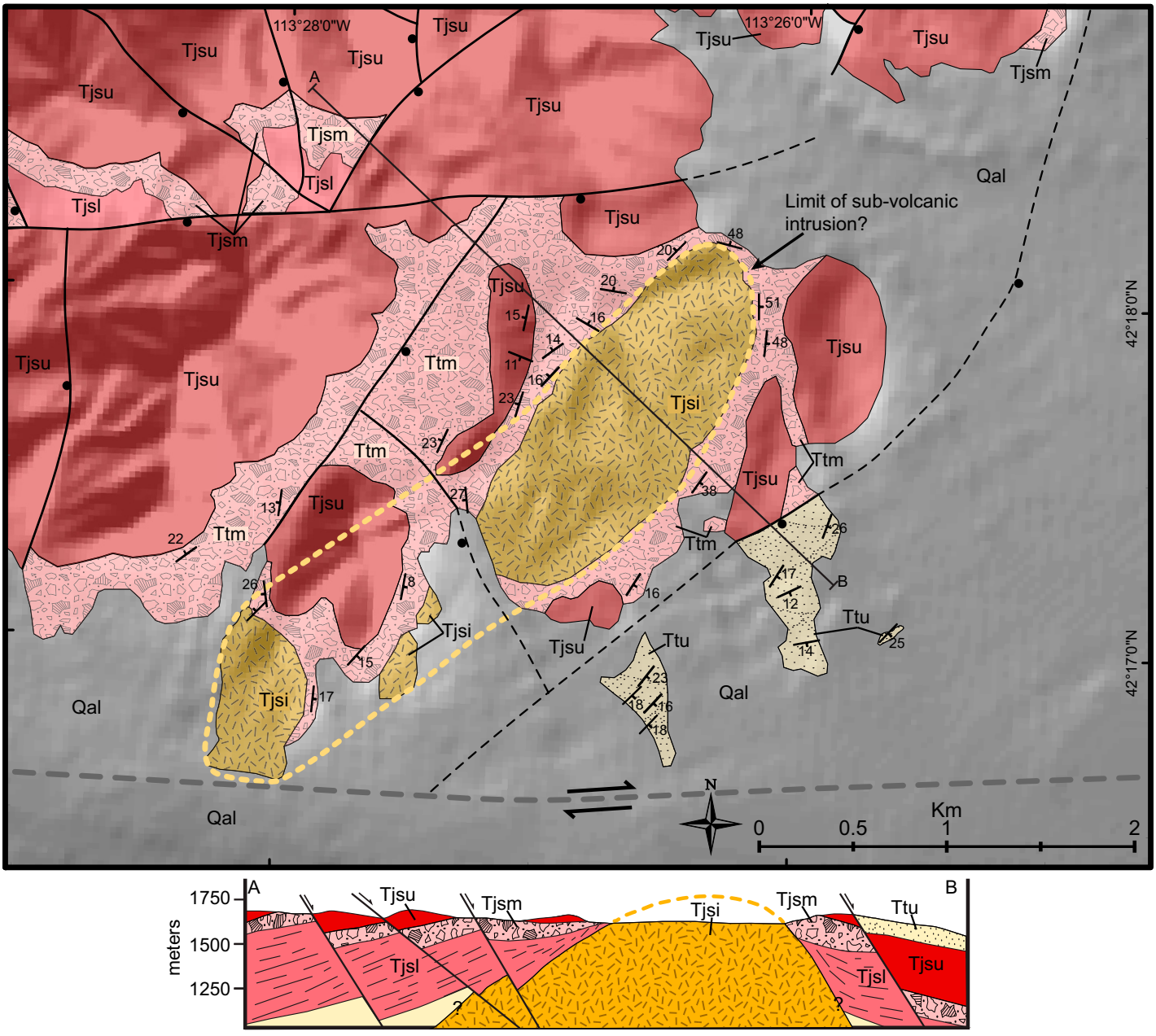


**Figure 5. Detailed map and cross section of the southern part of the Cotterel Mountains, showing the structural relationships of units around a subvolcanic intrusion. Note the radially dipping strata around the intrusive complex. Key is the same as in Figure 2. Abbreviations: Tjsl—lower member of the Jim Sage volcanic suite (JSVS); Ttm—middle sedimentary unit separating the members of the JSVS; Tjsu—upper member of the JSVS; Tjsi—subvolcanic intrusion; Ttu—Miocene tuff younger than the JSVS; Qal—Quaternary alluvium.**

Frantz magnetic separator). Zircon was hand-selected for final purity, mounted in a 25-mm-diameter epoxy disc, ground and polished to a 1 µm finish, and imaged in cathodoluminescence (Fig. 6) using a JEOL 5600 scanning electron microscope. U, Th, and Pb isotopes were measured on the SHRIMP-RG (using the procedure described in Strickland et al., 2011b), adjusting the count times for each isotope and the number of five scans (peak-hopping cycles from mass 156 through 270) to six to improve counting statistics for $^{206}$Pb and $^{207}$Pb, required to obtain Miocene ages with acceptable analytical precision (~1%–2% for individual analyses, 1σ).

The majority (n = 121) of zircons analyzed have concordant U-Pb ages, had low common Pb, and were interpreted as magmatic zircon that crystallized just prior to eruption of the volcanic rocks. The data were reduced using SQUID 1 (Ludwig, 2003) and concordia diagrams were constructed using Isoplot (Ludwig, 2003). Calculated ages for zircon are standardized relative to R33 (419 Ma; Black et al., 2004). The common Pb composition was based on the value reported by Stacey and Kramers (1975). The calculated concordia intercept ages (Fig. 7) and weighted average $^{207}$Pb-corrected $^{206}$Pb/$^{238}$U model ages are reported with 2σ errors (Table 1; Supplemental Table 1 [see footnote 1]). The weighted average ages of the five samples are

TABLE 1. SUMMARY INFORMATION OF SAMPLES FROM THIS STUDY

| Sample number | Unit | Description | Coordinates (deg. dec. deg.) N | W | Elevation (m) | Type of analysis M and T | U-Pb | Sr | Nd | $\delta^{18}O$ | Hf |
|---|---|---|---|---|---|---|---|---|---|---|---|
| JS-10-1 | lower member | rhyolite lava flow | 42.05053 | 113.45403 | 1629 | X | | | | X | X |
| JS-10 | lower member | rhyolite lava flow | 42.17989 | 113.42556 | | X | | X | X | | |
| JS-3 | lower member | rhyolite lava flow | 42.15872 | 113.48694 | 2048 | X | | | | | |
| JS-4 | lower member | rhyolite lava flow | 42.15975 | 113.49156 | 2041 | X | | X | | | |
| JS-5 | lower member | rhyolite lava flow | 42.15606 | 113.49378 | 2195 | X | | X | X | | |
| JS-6 | lower member | rhyolite lava flow | 42.15564 | 113.49314 | 2194 | X | | | | | |
| JS-7 | lower member | rhyolite lava flow | 42.15478 | 113.49261 | 2176 | X | | | | | |
| JS-8 | lower member | rhyolite lava flow | 42.15336 | 113.49000 | 2145 | X | | | | | |
| JS-9 | lower member | rhyolite lava flow | 42.15292 | 113.48814 | 2104 | X | | | | | |
| C-9A | lower member | rhyolite lava flow | 42.41295 | 113.58193 | 1443 | X | | | | | |
| C-11 | lower member | rhyolite lava flow | 42.33683 | 113.50008 | 1733 | X | | | | | |
| C-11B | lower member | rhyolite lava flow | 42.33683 | 113.50008 | 1733 | X | | | | | |
| JS-09-4 | lower member | rhyolite lava flow | 42.11627 | 113.51707 | 1939 | X | | | | | |
| JS-1 | lower member | rhyolite lava flow | 42.08495 | 113.49483 | 1846 | X | X | X | | | |
| JS-11B | lower member | rhyolite lava flow | 42.20290 | 113.42440 | 1591 | X | X | X | X | X | X |
| JS-11A | upper member | rhyolite lava flow | 42.20290 | 113.42440 | 1591 | X | | | | | |
| C-RA | upper member | rhyolite lava flow | 42.35344 | 113.46592 | 2000 | X | | X | | | X |
| C-RB | upper member | rhyolite lava flow | 42.35119 | 113.47703 | 1950 | X | | | | | |
| C-RC | upper member | rhyolite lava flow | 42.35119 | 113.47703 | 1950 | X | X | X | X | | |
| C-RD | upper member | rhyolite lava flow | 42.34325 | 113.48639 | 1916 | X | | X | X | | |
| C-RE | upper member | rhyolite lava flow | 42.33794 | 113.50256 | 1713 | X | | X | X | | |
| C-1A | upper member | rhyolite lava flow | 42.36008 | 113.45605 | 2159 | X | | | | | |
| C-1B | upper member | rhyolite lava flow | 42.36010 | 113.45607 | 2159 | X | X | X | | X | X |
| C-1C | upper member | rhyolite lava flow | 42.36012 | 113.45608 | 2159 | X | | | | | |
| C-8 | upper member | rhyolite lava flow | 42.51690 | 113.47520 | 1690 | X | | X | | | |
| C-9C | upper member | rhyolite lava flow | 42.41295 | 113.58193 | 1443 | X | | | | | |
| C-BA | upper member | basalt lava flow | 42.51242 | 113.49450 | 1430 | X | | X | | | |
| C-BB | upper member | basalt lava flow | 42.51675 | 113.48958 | 1489 | X | | X | | | |
| C-BC | upper member | basalt lava flow | 42.51706 | 113.48894 | 1493 | X | | X | X | | |
| C-7 | upper member | basalt lava flow | 42.51690 | 113.47520 | 1690 | X | | X | | | |
| C-10 | outflow | welded ignimbrite | 42.33713 | 113.49208 | 1858 | X | | | | | |
| JS-09-8B | outflow | welded Ignimbrite | 42.02977 | 113.59873 | 1639 | X | | | | | |
| JS-09-8C | outflow | rhyolite lava flow? | 42.02977 | 113.59873 | 1639 | X | | | | | |
| JS-09-2A | outflow | rhyolite lava flow? | 42.08718 | 113.48193 | 1813 | X | | | | | |
| JS-09-3A | outflow | rhyolite lava flow? | 42.07835 | 113.48597 | 1729 | X | | | | | |
| JS-09-7 | outflow | rhyolite lava flow? | | | | X | | | | | |
| C-4 | subvolcanic intrusion | silicified rhyolite | 42.29728 | 113.43872 | 1529 | X | | | | | |
| C-1 | subvolcanic intrusion | silicified rhyolite | 42.29203 | 113.44069 | 1529 | | X | | | | X |

*Note:* Datum for sample coordinates is NAD (North American Datum) 83. M and T—whole-rock major and trace element geochemistry; U-Pb—zircon U-Pb geochronology; Sr—whole-rock Sr isotope analyses; Nd—whole-rock Nd isotope analyses; $\delta^{18}O$—zircon oxygen isotope analyses; Hf—zircon Hf isotope analyses; deg. dec. deg.—degree decimal degree.

preferred as the inferred crystallization ages and are all within error of the concordia intercept ages. Zircon concentration data for U and Th were standardized against the well-characterized, homogeneous zircon standard MAD-green (Barth and Wooden, 2010).

## Whole-Rock Major and Trace Element Geochemistry

We selected 37 samples for whole-rock major and trace element analyses (Table 1; Fig. 8; Supplemental Table 2[2]), 15 samples from the lower member of the JSVS, 11 from the upper member, and 6 samples of ignimbrite and lava, the stratigraphic positions of which with respect to the JSVS rhyolite flows are not certain due to lack of continuous exposure (outflows). In addition, four samples of the basalt of Cotterel were analyzed. The samples were analyzed using X-ray fluorescence at Washington State University (Pullman, Washington, USA; 13 samples) and Macalester College (St. Paul, Minnesota, USA; 24 samples); 13 samples were dissolved and analyzed for trace and rare earth elements using inductively coupled plasma–mass spectrometry (ICP-MS) at Washington State University (Fig. 9). Analyses of 12 additional samples of Precambrian basement rocks are also included in Figure 8 (compiled from Egger et al., 2003; Strickland et al., 2011b; Konstantinou et al., 2013).

## Electron-Microprobe Phenocryst Geochemistry

Three samples from the lower (JS-3, JS-7, JS-10) and three from the upper member (C-RA, C-RD, C-RE) of the JSVS were selected for electron-microprobe analyses of phenocryst chemistry assemblages (Fig. 10; Supplemental Table 3[3]) using the JEOL JXA-733A electron probe at Stanford University (Stanford, California). Pyroxene and feldspar phenocrysts were selected and analyzed for the abundance of major element oxide compositions. The oxide abundances were standardized using well characterized in-house mineral standards and the results were normalized to six oxygen atoms for pyroxene and eight for feldspar (Supplemental Table 3 [see footnote 3]).

## Isotope Geochemistry

We selected 15 samples from the JSVS for whole-rock Sr and a subset of 7 samples for Nd analyses performed at the Stanford ICP-

[2]Supplemental Table 2. Whole-rock major and trace element data of Miocene volcanic rocks of the Jim Sage volcanic suite determined by X-ray fluorescence and dissolution inductively coupled plasma–mass spectrometry. If you are viewing the PDF of this paper or reading it offline, please visit http://dx.doi.org/10.1130/GES00948.S2 or the full-text article on www.gsapubs.org to view Supplemental Table 2.

[3]Supplemental Table 3. Electron-microprobe major element compositions of feldspar and pyroxene phenocryst assemblages from the Jim Sage volcanic suite. If you are viewing the PDF of this paper or reading it offline, please visit http://dx.doi.org/10.1130/GES00948.S3 or the full-text article on www.gsapubs.org to view Supplemental Table 3.

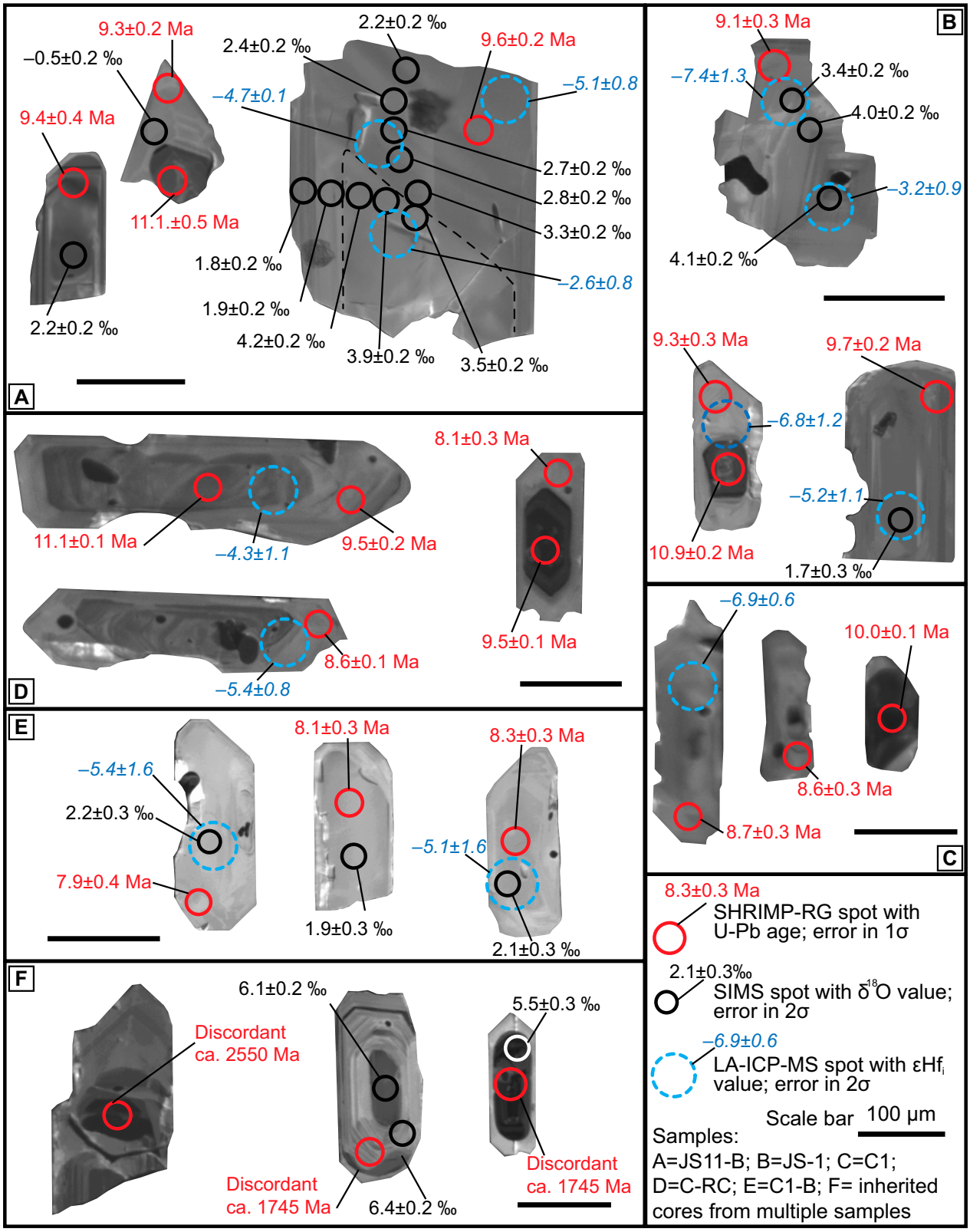


**Figure 6. Diagram showing representative cathodoluminescence images of zircons from the igneous rocks dated in this study showing the spot analyses for U-Pb geochronology, oxygen isotope analyses, and Hf isotope analyses. Red circles indicate the spots where $^{207}Pb$-corrected $^{206}Pb/^{238}U$ ages obtained from SHRIMP-RG (sensitive high-resolution ion-microprobe–reverse geometry) analyses, black circles indicate the spots analyzed for oxygen isotope compositions by secondary ion mass spectrometer (SIMS), and blue circles indicate spot locations from Hf isotope analyses by LA-ICP-MS (laser ablation–inductively coupled plasma–mass spectrometry). Black scale bar is 100 µm for all the samples.**

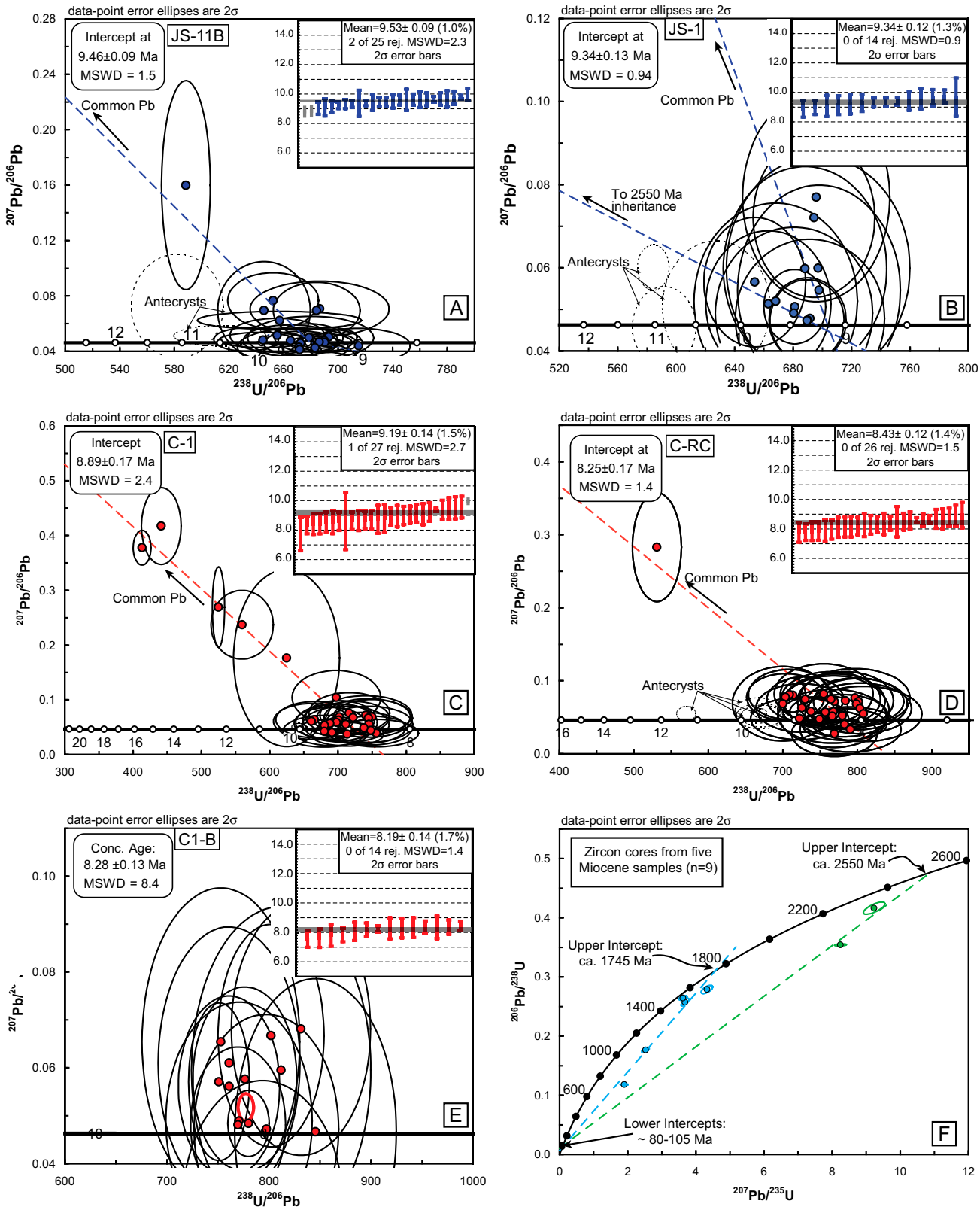


**Figure 7. (A–E) Concordia diagrams and weighted averages for the samples dated in this study. The intercept or concordia ages are indicated for each sample, as well as the weighted average age of the $^{207}Pb$-corrected $^{206}Pb/^{238}U$ ages for each sample (MSWD—mean square of weighted deviates). Dashed ellipses are interpreted as antecrystic or inherited zircon and were not included in the weighted mean calculation. (F) Concordia diagram showing the distribution of inherited zircon grains from the Jim Sage volcanic suite (JSVS). The inherited grains fall into two general age groups (ca. 1754 Ma, shown in blue and 2550 Ma, shown in green) and along their discordia with Mesozoic lower intercepts (ca. 105 and 80 Ma).**

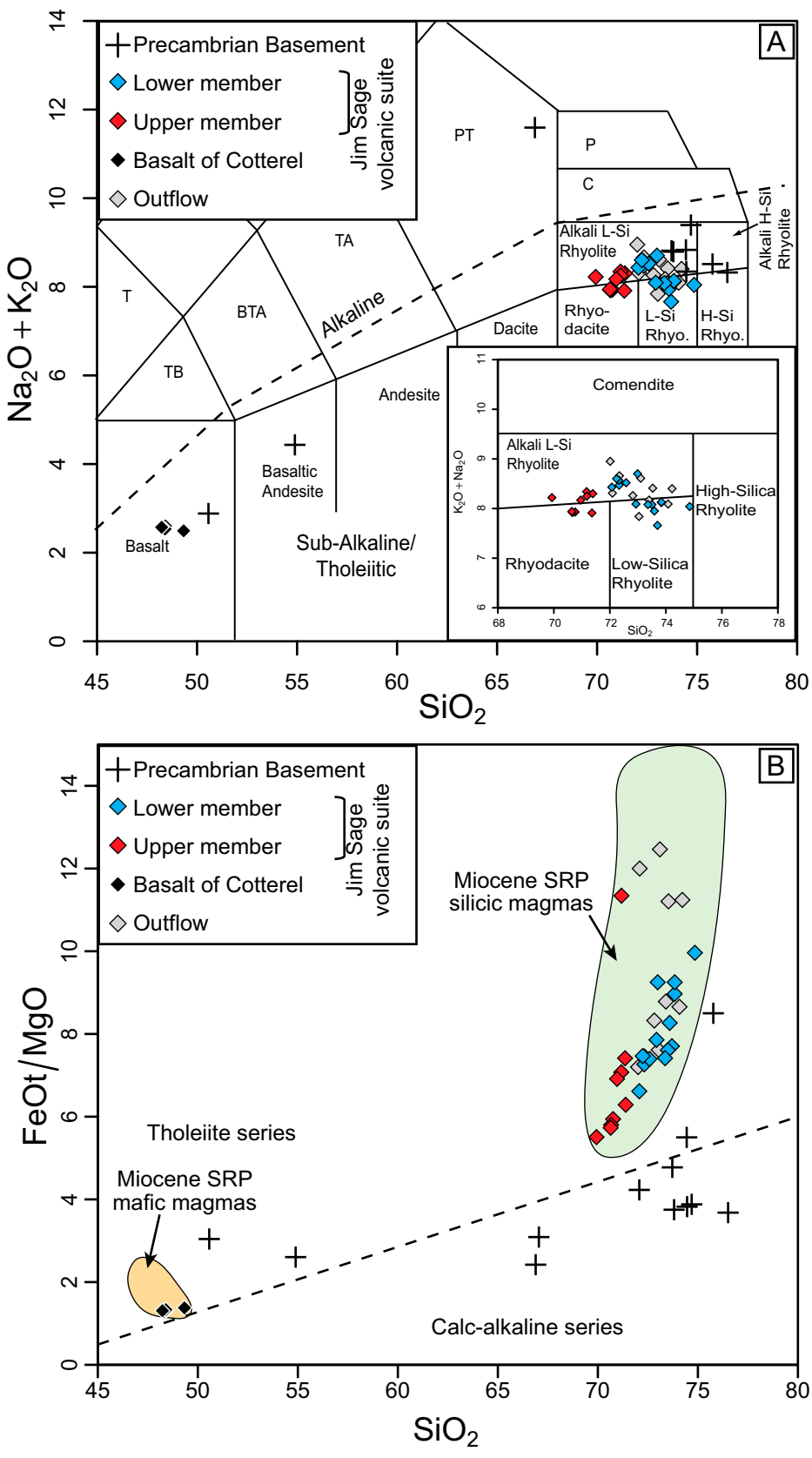


**Figure 8. Whole-rock major element compositions of samples from the Jim Sage volcanic suite (JSVS), basalt of Cotterel Mountains (Williams et al., 1982), of outflow samples with poorly constrained stratigraphic position, and Precambrian igneous rocks from the Albion–Raft River–Grouse Creek metamorphic core complex. (A) Total alkali versus silica (G. Mahood, 2013, personal commun.) diagram indicating the range of compositions of the JSVS and igneous rocks of the Precambrian basement (used as models for crustal sources). Abbreviations: BTA—Basaltic trachyandesite; C—Comendite; H-Si—high silica; L-Si—low silica; PT—Phono-tephrite; P—Phonolite; Rhyo.—rhyolite; T—Trachyte; TA—Trachyandesite; TB—Trachybasalt. (B) FeOt/MgO versus $SiO_2$ diagrams of the same suite of rocks. Fields for Snake River Plain (SRP) basalt and rhyolite are from Christiansen and McCurry (2008).**

MS-TIMS (thermal ionization mass spectrometry) facility (Table 1; Fig. 11; Supplemental Table 4[4]). For more details about the procedures used for sample dissolution and mass spectrometry, see Appendix 1.

The O isotope compositions of individual zircon domains, dated by SHRIMP-RG (n = 70), from three samples (JS1, JS11-B, C1B) were determined in situ using an IMS-1280 at the University of Wisconsin WiscSIMS (Wisconsin Secondary Ion Mass Spectrometer) laboratory following the procedures described in Kita et al. (2009) and Valley and Kita (2009), and $\delta^{18}O$ (Vienna standard mean ocean water, VSMOW) values were calculated with precision reported at 2 standard deviation (SD) level (see Appendix 2 for details of the method; Fig. 12A; Supplemental Table 5[5]). A $^{133}Cs^+$ beam was focused to ~10 µm spots and secondary ions of $^{18}O$ and $^{16}O$ were counted with dual Faraday cup detectors. Groups of ~10 sample

[4]Supplemental Table 4. Whole-rock Sr and Nd isotope results from Miocene volcanic rocks of the Jim Sage volcanic suite. If you are viewing the PDF of this paper or reading it offline, please visit http://dx.doi.org/10.1130/GES00948.S4 or the full-text article on www.gsapubs.org to view Supplemental Table 4.

[5]Supplemental Table 5. Results of zircon oxygen isotope analyses, performed at the WiscSIMS (University of Wisconsin, Wisconsin Secondary Ion Mass Spectrometer) facility. If you are viewing the PDF of this paper or reading it offline, please visit http://dx.doi.org/10.1130/GES00948.S5 or the full-text article on www.gsapubs.org to view Supplemental Table 5.

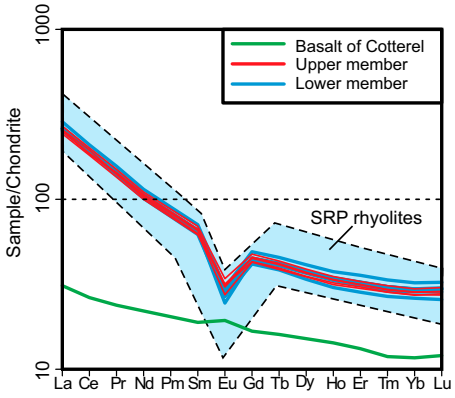


**Figure 9. Whole-rock chondrite-normalized rare earth element spider diagram of the rhyolite lavas of the Jim Sage volcanic suite and the flows of the basalt of Cotterel Mountains (Williams et al., 1982). Chondrite normalization after Boyton (1985). Snake River Plain (SRP) rhyolite data are from Ellis et al. (2013).**

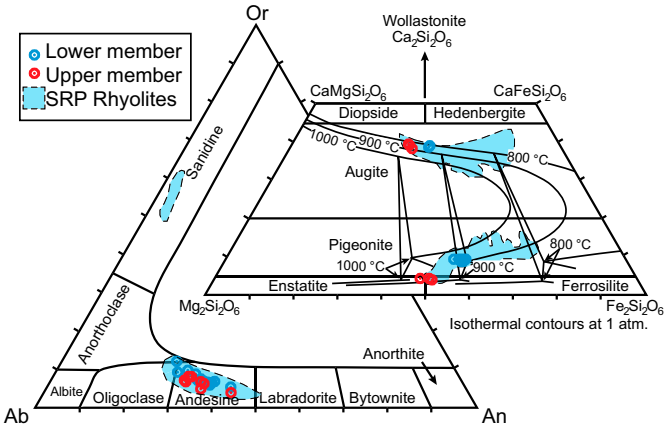


**Figure 10. Ternary diagrams for feldspar (anorthoclase-albite-orthoclase) and pyroxene (Fe- enstatite-wollastonite), showing the compositions of phenocryst assemblages from the lower and upper members of the Jim Sage volcanic suite. Snake River Plain (SRP) rhyolite data are from Ellis et al. (2013).**

analyses were bracketed by a total of at least 8 analyses of KIM-5 zircon standard (Valley 2003), which are used to correct for instrument bias. The average value of bias was –0.31‰ and ranged from –0.10‰ to –0.54‰. The reproducibility of these groups of standard data, which varied from 0.19 to 0.52, permil ‰ is considered the best indication of analytical precision, and is reported at 2 SD. For the purpose of this study, we have used the $\delta^{18}O_{zr}$ (zr—zircon) values to calculate $\delta^{18}O_{wr}$ using the equation rearranged from Lackey et al. (2008): $\delta^{18}O_{wr} \approx \delta^{18}O_{zr} + 0.0612\ (wt\%\ SiO_2) - 2.5$.

Hf isotopic compositions were determined in situ on the same zircons that were dated and analyzed for O isotope compositions, from five samples of the JSVS (n = 56). The analyses were performed at Washington State University's LA-ICP-MS facility (LA—laser ablation), following the procedure of C.M. Fisher (2013, personal commun.); for detailed methods, see Appendix 3. Individual zircon crystals from two lower member samples (samples JS11-B, JS-1), two upper member samples (C1B, C-RC), and a subvolcanic intrusion sample (sample C1) were analyzed (Fig. 12B; Supplemental Table 6[6]).

[6]Supplemental Table 6. Results of zircon Hf isotope analyses, performed at the Washington State University laser ablation–inductively coupled plasma–mass spectrometry facility. If you are viewing the PDF of this paper or reading it offline, please visit http://dx.doi.org/10.1130/GES00948.S6 or the full-text article on www.gsapubs.org to view Supplemental Table 6.

## RESULTS

### Stratigraphy of the Jim Sage Volcanic Suite

Distinguishing between high-temperature rheomorphic ignimbrites and rhyolite lavas that erupted from the SRP is challenging because the intense welding of these ignimbrites gives them a lava-like appearance (Branney et al., 2008). Differentiating between individual ignimbrite units is equally difficult due to their similar appearance and geochemistry (e.g., Hildreth and Mahood, 1985). Many workers have used high-precision geochronology, trace element geochemistry, and phenocryst geochemistry to correlate individual ignimbrite units and estimate the volumes of individual eruptions (e.g., Hildreth and Mahood, 1985; Bonnichsen et al., 2008; Ellis et al., 2012). In this study, we used the physical characteristics of the volcanic deposits (thickness, aspect ratios, terminations of the flows and basal contacts; outlined by Branney et al., 2008) to differentiate between lavas and ignimbrites in the JSVS.

The rhyolite flows of the JSVS are exposed along two north-south elongate antiformal structures that make up the rugged Jim Sage and Cotterel Mountains (Fig. 2). The JSVS is composed of two members separated by a thin sequence of sediments (Fig. 3). A dark weathering, moderately to densely welded ignimbrite is exposed in the Raft River Basin, ~10–11 km southwest of the Jim Sage Mountains, but these exposures are separated by alluvial cover from the lava flows exposed at the Jim Sage Mountains (Fig. 3). The base of the lower member overlies fine-grained lacustrine deposits of the Salt Lake Formation (Konstantinou et al., 2012; Fig. 3). Underlying sedimentary rocks locally preserve evidence of soft-sediment deformation and high-temperature fusion at the contact with the lower rhyolite lava flow (Fig. 3). The two members have nearly constant thickness (370–440 m for each member) along their strike length, except at their northern and southern exposures, where they taper rapidly and have ~30–50-m-thick terminal lobes. The two members are exposed over areas of ~260 km$^2$ and have aspect ratios between 1:40–1:50, and calculated volumes, based on cross sections and map patterns, ranging from 110 to 130 km$^3$ (Fig. 2).

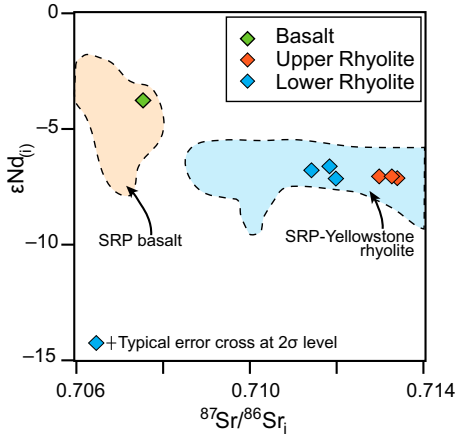


**Figure 11. Results of whole-rock Sr and Nd isotope analyses from selected samples of the Jim Sage volcanic suite and the basalt of Cotterel Mountains (Williams et al., 1982). The range of isotopic values from the Snake River Plain (SRP) and Yellowstone province is from Christiansen and McCurry (2008).**

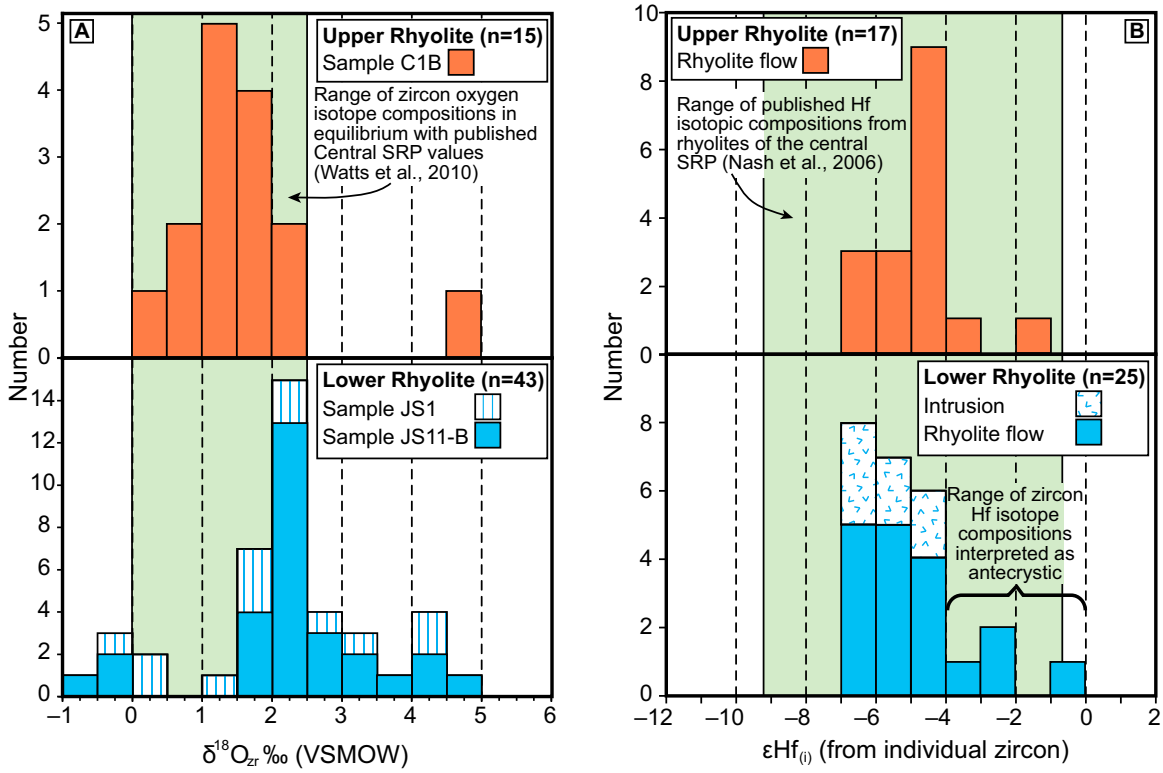


**Figure 12. (A) Summary of $\delta^{18}O_{zr}$ (zr—zircon) compositions from the lower and upper member of the Jim Sage volcanic suite (JSVS) obtained from analyses of individual zircon domains. Also shown is the range for the central Snake River Plain (SRP) as estimated from whole-rock values reported in Watts et al. (2010). VSMOW—Vienna standard mean ocean water. (B) Summary of $\varepsilon_{Hf(i)}$ compositions from zircon of the upper and lower member of the JSVS obtained from analyses of individual zircon domains. SRP values are from glass shards of different units reported in Nash et al. (2006).**

The lower member is best exposed in the canyons along the eastern side of the Jim Sage Mountains (Fig. 2). The base of the member consists of a 5–30-m-thick rhyolitic autobreccia, with vitreous clasts and a matrix of strongly altered glass (Figs. 3, 4A, and 4G). The rest of the lower member is made up of a thick (350–400 m) sequence of massive or layered, glassy rhyolite lava with occasional columnar jointing and devitrified interiors (Fig. 3). These rocks have aphanitic or glassy matrix and 20%–25% phenocrysts of euhedral plagioclase (andesine) > anhedral augite and pigeonite > Fe-Ti oxides > quartz > sanidine >> zircon, and are similar to the phenocryst compositions of rhyolite erupted from the SRP province (e.g., Bonnichsen and Citron, 1982; Honjo et al., 1992; Andrews et al., 2008; Ellis and Wolff, 2012; Fig. 4A).

The lower and upper members are separated by a relatively thin (0–100 m) sedimentary breccia containing clasts derived from the underlying lower member (Fig. 3). The breccia is topped by a ~50–100-m-thick lacustrine sedimentary unit composed of thickly bedded calc-arenite and tuff, with thin beds of volcanic sandstone composed of glass shards (Fig. 3).

The upper member is best exposed in the Cotterel Mountains, and has a locally autobrecciated base with occasional peperites and clasts of the older rhyolite lavas (Figs. 3 and 4E). The peperites provide evidence that the lavas flowed in water or wet sediment. The majority of the upper member is made up of ~400 m of intercalated massive and banded lava with thick sequences characterized by columnar joints (Fig. 3). These lavas are similar in appearance to the lower member unit, with aphanitic or glassy matrix and 20%–25% phenocrysts composed of euhedral plagioclase (andesine) > anhedral augite and pigeonite > Fe-Ti oxides > quartz > sanidine >> zircon (Figs. 4B, 4E, 4F). Thus, the basal contacts of both the lower and upper member are characterized by autobreccias, typical of silicic lavas, rather than a basal surge deposit characteristic of a welded ignimbrite (Branney et al., 2008; Figs. 4A, 4B, 4E–4G). The thicknesses (lack of exposures with thickness of <30 m), aspect ratios, and abrupt lobate terminations are all consistent with the physical attributes of silicic lava flows of the SRP (Branney et al., 2008; Fig. 2). In addition, based on seismic reflection data and borehole data, it was demonstrated (Konstantinou, 2013) that these rhyolites are not widely present in the Raft River Basin, buried beneath younger sediments. Instead, the eastern limit of the rhyolite flows is their approximate present-day exposure in the Jim Sage and Cotterel Mountains. Had these rhyolite flows been ignimbrites, one would expect they would have spread out more thinly to fill the east-west extent of the floor of the Raft River Basin, but the rhyolites were not sampled in the deep boreholes of the Raft River Basin that penetrated the lower plate of the metamorphic core complex (Williams et al., 1974, 1982; Covington, 1983).

Small subvolcanic intrusions (vents) and lava domes are also present. These are identified by their silicified interiors, and the fact that they dome the strata they were intruded into (Figs. 2 and 5). Based on a positive magnetic anomaly that covers the area of exposed rhyolite domes (Fig. 2) and on seismic reflection profiles that image what appear to be intrusions (Mabey and Wilson, 1973; Williams et al., 1974, 1982; Cov-

ington, 1983; Konstantinou, 2013), an elliptical (~4 by 2 km) cryptodome probably underlies the eastern portion of the Jim Sage Mountains (Fig. 2). We infer the exposed domes and the cryptodome to be part of the vent system for the lavas of the JSVS.

Above the upper rhyolite member of the JSVS is a thin (<100 m), densely welded ignimbrite with an interior zone that displays intense rheomorphic flow and transposed and/or deformed shards (Fig. 4C). A less welded distal phase of this ignimbrite preserves small collapsed pumice lapilli (Figs. 4C, 4D). This ignimbrite covers most of the northern Cotterel Mountains, forming a relatively smooth dip slope on its northwestern side (Fig. 2). The ignimbrite is also exposed in the hills near the town of Albion (Fig. 2). Above this ignimbrite is a capping sequence of basaltic flows exposed in the northern Cotterel Mountains (basalt of Cotterel Mountains of Williams et al., 1982), which is as much as ~100 m thick, and was dated as 9.2 ± 1.5 Ma (1σ; K-Ar; Armstrong et al., 1975). Both the ignimbrite and the basalt of Cotterel are inferred to be erupted from the central SRP.

Lacustrine sediments conformably overlie the upper rhyolite flow, are poorly exposed along the flanks of the Cotterel Mountains, and are known from borehole localities in the eastern part of the Raft River Basin (Fig. 4). These deposits consist mostly of thick-bedded reworked ash-fall tuffs and marls and contain clasts of rhyolite from the JSVS.

## SHRIMP-RG U-Pb Geochronology of Zircon

Sample JS11-B, from the lower member of the JSVS, is a two-pyroxene rhyolite lava containing euhedral zircon (Fig. 6A). The weighted mean of 23 $^{207}$Pb-corrected $^{206}$Pb/$^{238}$U ages yields an age of 9.53 ± 0.10 Ma (2σ) with a mean square of weighted deviates (MSWD) of 2.3 (Fig. 7A). Zircon analyses (n = 14) from a second sample, collected from a higher stratigraphic position of the lower member of the JSVS (sample JS1), yielded a weighted mean age of 9.34 ± 0.12 Ma (2σ; MSWD = 0.9; Fig. 7B). Three zircon grains resulted in slightly older U-Pb ages (ca. 10–11 Ma) and are interpreted as antecrystic (e.g., Bindeman et al., 2001). Sample C1, collected from the subvolcanic intrusion in the southern Cotterel Mountains, yields a weighted mean age of 9.19 ± 0.14 Ma (2σ; MSWD = 2.7; n = 26). The high MSWD may reflect two zircon populations with an irresolvable age difference (Fig. 7C).

Two samples from the upper member of the JSVS were also collected and dated. Sample C-RC is a two-pyroxene rhyolite lava that yielded a weighted mean age of 8.43 ± 0.12 Ma (2σ; MSWD = 1.5; n = 26; Fig. 7D). Four zircon grains resulted in slightly older ages (ca. 9.5 and 11 Ma) and are interpreted to be antecrystic, similar to observations from the Yellowstone caldera (Vazquez and Reid, 2002). A second, very similar sample collected from a higher stratigraphic position (C1B) yielded a weighted mean age of 8.19 ± 0.14 Ma (2σ; MSWD = 1.4; n = 14; Fig. 7E).

A small number of zircon cores (n = 9) from all five Miocene samples were identified and dated; these ages are plotted on the same concordia diagram (Fig. 7F). U-Pb isotope ratios from individual zircon define two discordia lines with poorly constrained upper intercepts ca. 2550 and 1745 Ma (±140–150 m.y.) and Mesozoic lower intercepts (ca. 75 and 95 Ma ± 270 m.y.; Fig. 7F). These data points are too few for any conclusive interpretation, but there are widespread exposures of Archean basement in the region dated as ca. 2550 Ma, and most Eocene–Oligocene plutons of the Albion–Raft River–Grouse Creek metamorphic core complex that have been studied have similar inherited ages (Strickland et al., 2011b; Konstantinou et al., 2011, 2013).

## Results from Major and Trace Element Geochemistry

The lower member of the JSVS has a limited range in composition, varying from low-silica alkali rhyolite to low-silica rhyolite ($SiO_2$ = 72%–74%; Fig. 8). The upper member of the JSVS is a low-silica alkali rhyolite with slightly less silica content ($SiO_2$ = 70%–71.5%; Fig. 8) than the lower member. The four mafic samples are basaltic in composition and most of the outflow ignimbrite and lava samples (away from the Jim Sage and Cotterel Mountains) have compositions similar to that the lower member of the JSVS (Fig. 8). All of the JSVS samples are ferroan (high $FeO_t$/MgO ratios), and distinctly different from the evolved calc-alkalic composition of the underlying Archean basement in the region (Fig. 8B). The rare earth element (REE) patterns of the rhyolite samples from the lower and upper members of the JSVS are very similar, and show strong enrichment in light (L) REEs relative to heavy (H) REEs, and large negative Eu anomalies (Fig. 9). The basalt of Cotterel Mountains has a small enrichment in LREEs relative to HREEs and a small positive Eu anomaly (Fig. 9).

## Geochemistry of Phenocryst Assemblages

The lower and upper rhyolite members of the JSVS have andesine feldspar phenocrysts that are homogeneous in composition (Fig. 10). The two members of the JSVS have distinctly different pyroxene pair compositions. The lower member is characterized by an augite-pigeonite pyroxene pair, and the upper member of the JSVS has an augite-pigeonite pair that contains more MgO than the lower member (Fig. 10). The pyroxene pairs in the rhyolite lavas are consistent with being in equilibrium at high temperatures (~850–900 °C; Lindsley, 1983) and low pressures (<3 kbar), and are similar to typical central SRP rhyolites (e.g., Bonnichsen and Citron, 1982; Honjo et al., 1992; Andrews et al., 2008; Ellis et al., 2010). In addition, a single population of augite and pyroxene pair in both flow units is consistent with similar observations of central SRP lavas, whereas ignimbrites from the province often have multiple populations of pyroxene pairs (Cathey and Nash, 2009; Ellis and Wolff, 2012).

## Whole-Rock Multicollector-ICP-MS Sr and Nd Isotope Analyses

The whole-rock Sr and Nd isotope results were used to calculate age-corrected $^{87}$Sr/$^{86}$Sr$_i$ and $\varepsilon_{Nd(i)}$ values (Fig. 11; Supplemental Table 4 [see footnote 4]; Bouvier et al., 2008). The lower member has $^{87}$Sr/$^{86}$Sr$_i$ = 0.7114–0.7121 and $\varepsilon_{Nd(i)}$ values that range from –6.7 to –7.1; the upper member has $^{87}$Sr/$^{86}$Sr$_i$ = 0.7130–0.7135 and $\varepsilon_{Nd(i)}$ values of –7.1 (Fig. 11). The basalt of Cotterel Mountains has $^{87}$Sr/$^{86}$Sr$_i$ composition of 0.7066–0.7075 and $\varepsilon_{Nd(i)}$ = –3.7 (Fig. 11; Supplemental Table 4 [see footnote 4]). The isotopic compositions of the rhyolite lavas of the JSVS and the basalt of Cotterel Mountains are very similar to published data from rhyolites and basalts of the central SRP (Fig. 11; Nash et al., 2006; Christiansen and McCurry, 2008).

## In Situ Zircon Secondary Ion Mass Spectrometer O Isotope Analyses

The O isotope compositions of individual analytical spots from Miocene JSVS zircons from the lower member range in $\delta^{18}O_{zr}$ (VSMOW) from –0.5‰ to 4.6‰, and from the upper member range from 0.5‰ to 4.9‰ (Fig. 12A; Supplemental Table 5 [see footnote 5]). However, most of the zircon analyses cluster around values of $\delta^{18}O_{zr}$ (VSMOW) ranging from 0‰ to 2.5‰ (43 of 58 analyses), with only one analysis having a $\delta^{18}O_{zr}$ value >5‰. The whole-rock oxygen isotope compositions calculated from $\delta^{18}O_{zr}$ range from $\delta^{18}O_{wr} \approx$ 6.7‰ to 1.4‰ (but mostly cluster around 2‰–4.5‰) and are similar to values reported from the 12–6 Ma rhyolites of the central SRP (see compilation in Watts et al., 2010; Fig. 12A). A few large (~200 µm in diameter) zircon grains were analyzed with multiple

secondary ion mass spectrometer spots, and the results show isotopic zoning within individual grains (Figs. 6A, 6B). In this limited number of examples, we observed a decrease in $\delta^{18}O_{zr}$ from core ($\delta^{18}O_{zr}$ ~ 4‰) to rim ($\delta^{18}O_{zr}$ ~ 2.2‰), similar to observations from Yellowstone zircon reported in Bindeman et al. (2008).

### In Situ Zircon LA-ICP-MS Hf Isotope Analyses

The Hf isotope results and the calculated $\varepsilon_{Hf_{(i)}}$ values from the upper and the lower members of the JSVS are summarized in Figure 12B (Supplemental Table 6 [see footnote 6]). The Hf isotope analyses yielded zircon $\varepsilon_{Hf_{(i)}}$ values ranging from –0.8 to –6.8, but most of the analyses have a small range from ~–4 to –6.5 and the values obtained from each individual sample are homogeneous (Fig. 12B; Supplemental Table 6 [see footnote 6]). The lower member of the JSVS has zircon $\varepsilon_{Hf_{(i)}}$ values that range from –0.8 to –6.8, and the upper member has a range of values from –1.6 to –6.6 (Fig. 12B). The total range of values within each unit is larger than the 2σ error on individual zircon analysis (±1.5 $\varepsilon_{Hf}$ units). Zircons with $\varepsilon_{Hf_{(t)}}$ values from –0.8 to –2.1 are suggested to be antecrystic because they have Hf isotope compositions that are more radiogenic than the majority of zircon analyses, which cluster around –4 and –6.5 $\varepsilon_{Hf_{(t)}}$ values (Fig. 12B).

### Possible Crustal and Mantle Sources for Geochemical Modeling

Based on stratigraphic considerations alone, the Albion–Raft River–Grouse Creek metamorphic core complex represents a relative vertical uplift of a minimum of 10 km, from the top of the Paleozoic section to the Archean (Konstantinou et al., 2012). Thus the metamorphic core complex exposes extensive areas of once deep-seated rocks, similar to those that may underlie the central SRP and the JSVS. The Sr-Nd-Hf-O isotope compositions of several igneous and metamorphic rocks of different ages now exposed in the core complex are well characterized (Strickland et al., 2011b; Konstantinou et al., 2013). Here we summarize the stratigraphy and the crustal structure of rock units currently exposed in the Albion–Raft River–Grouse Creek metamorphic core complex. Because of their regional nature, these same rock units might be expected to be at depth beneath the SRP and southern Idaho. The highest stratigraphic and/or structural levels compose a thick (6–8 km) sequence of Paleozoic carbonates now partly exposed in the Black Pine Mountains (Fig. 1; Compton et al., 1977) and in mountain ranges surrounding the Albion–Raft River–Grouse Creek metamorphic core complex. It is unlikely that this upper part of the crust would be involved as a major source of contamination for Miocene magmas, because it is not thermodynamically favorable to melt and assimilate carbonate rocks in igneous systems. A thick sequence (~5 km) of Neoproterozoic quartzites and schists is beneath this carbonate sequence and constitutes the base of the passive margin succession of western North America. Even though these rocks have been tectonically attenuated (to ~1 km) in the Albion–Raft River–Grouse Creek metamorphic core complex (Fig. 1), they are probably thicker to the north (e.g., Compton et al., 1977; Compton 1972, 1975), and may have underlain extensive areas of southern Idaho. The schist units have compositions favorable for having undergone partial melting during Miocene magmatism. The structurally deepest and oldest rocks exposed today in the metamorphic core complex are Archean crystalline rocks of the Green Creek Complex, which constitutes depositional basement for the Neoproterozoic and Phanerozoic cover sequence. The Green Creek Complex is composed primarily of augen orthogneiss with lesser amphibolite, diorite, tonalite, and metasedimentary rocks (e.g., Compton, 1972, 1975), all of which have favorable compositions to undergo melting during Miocene magmatism. Rocks of similar Archean age and isotopic composition have been incorporated as xenoliths in basaltic magma of the SRP (Leeman et al., 1985). Finally the Albion–Raft River–Grouse Creek metamorphic core complex exposes a wide variety of Eocene–Oligocene calc-alkaline plutons that also have compositions favorable to undergo melting during Miocene magmatism. Similar Eocene plutons are exposed in the Challis volcanic field (e.g., Criss and Taylor, 1983; Criss et al., 1984), and the extensive magmatic roots of these Cenozoic plutons may underlie large areas of southern Idaho, including the region of the SRP province.

For the purpose of modeling the petrogenesis of the Miocene magmas (see following discussions), we made some simplifying assumptions about possible crustal reservoirs, assuming average isotopic compositions of the lower crust, upper crust, and a mantle source for the magmatic system (following the reasoning in Konstantinou et al., 2013) and summarized in the following. However, the structure and composition of the deep crust are likely more variable and complex than assumed here and shown in Table 2 and Figure 13.

Silicic rocks like the Proterozoic schist units, the Archean orthogneiss and the Eocene–Oligocene plutons that intrude them, are the dominant rock type exposed in the Albion–Raft River–Grouse Creek metamorphic core complex (e.g., Egger et al., 2003; Strickland et al., 2011b; Konstantinou et al., 2013). We infer that similar rocks may underlie the whole region of southern Idaho, and we collectively refer to these potential sources and/or contaminants as upper crust (Fig. 13; Table 2). Specifically, we used the composition of Oligocene plutons to represent the composition of the upper crust reservoir. The bulk Sr-Nd isotopic composition of the upper crust was estimated to be $^{87}Sr/^{86}Sr_{10}$ = 0.716, and $\varepsilon_{Nd_{(10)}}$ = –28 based on measured values from the Oligocene plutons (Table 2; Strickland et al., 2011b; Konstantinou et al., 2013; Fig. 13A). The $\varepsilon_{Hf_{(10)}}$ of the potential upper crust reservoir was estimated to be $\varepsilon_{Hf_{(10)}}$ = –32, based on values obtained in zircon from Oligocene magmas in the Albion–Raft River–Grouse Creek metamorphic core complex (Konstantinou et al., 2013; Table 2). The values selected for $\varepsilon_{Hf_{(10)}}$ and $\varepsilon_{Nd_{(10)}}$ do not follow the terrestrial array relationship established by Vervoort et al. (2011), but are based on the measured isotopic ratios of Oligocene plutons. Zircon $\delta^{18}O$ values analyzed from the Oligocene plutons and the Archean basement were used to estimate whole-rock magmatic values. These calculated $\delta^{18}O_{wr}$ for the Archean and Oligocene rocks have a very narrow range of 6.5‰–7.5‰, with an average value of $\delta^{18}O_{wr}$ = 7.1‰ (Konstantinou et al., 2013). However the $\delta^{18}O_{wr}$ of the upper crustal potential crustal reservoir was estimated to be either –1.5‰, similar to values estimated for the SRP (e.g., Watts et al., 2011), or ~2.5‰, similar to values measured from hydrothermally altered rocks of the Idaho batholith (Criss and Taylor, 1983; Criss et al., 1984). This low-$\delta^{18}O_{wr}$ value reflects postmagmatic hydrothermal alteration by meteoric waters in the region of southern Idaho. The cause of this alteration discussed in the following.

Eocene plutons in the Albion–Raft River–Grouse Creek metamorphic core complex are thought to have extensive deep roots, which are not exposed, based on the time span of Eocene magmatism and the compositions of these plutons (Konstantinou et al., 2013). In addition, the Archean basement is inferred to include rocks of more mafic compositions at depth, based on the isotopic composition of the Cenozoic igneous rocks (Strickland et al., 2011b; see detailed discussion in Konstantinou et al., 2013). A potential lower crust reservoir could be represented by the roots of Eocene plutons as well as by intermediate-composition Archean crystalline rocks. Based on the interpretation (made in Konstantinou et al., 2013) that the Eocene plutons in the Albion–Raft River–Grouse Creek metamorphic core complex represent reworking of the deep crust, we assume that the isotopic

TABLE 2. PARAMETERS USED IN ASSIMILATION–FRACTIONAL CRYSTALLIZATION MODELING OF THE JIM SAGE VOLCANIC SUITE, INCLUDING THE COMPOSITIONS OF THE DIFFERENT CRUSTAL AND MANTLE RESERVOIRS

| Reservoirs | $Sr_i$ | Sr (ppm) | Bulk D Sr | $\varepsilon_{Nd}$ | Nd (ppm) | Bulk D Nd | $\varepsilon_{Hf}$ | Hf (ppm) | Bulk D Hf | $\delta^{18}O_{WR}$ | Δ |
|---|---|---|---|---|---|---|---|---|---|---|---|
| | Stage I: Assimilation of basalt and mafic lower crust (r = 0.96) | | | | | | | | | | |
| Average mantle (pristine magma I) | 0.7053 | 135 | 0.1 | 2.0 | 11.5 | 0.1 | 5.0 | 2.5 | 0.1 | 5.6 | –0.2 |
| Lower crust | 0.7108 | 450 | 0.1 | –18.0 | 30.0 | 0.1 | –22.0 | 3.5 | 0.1 | 7.0 | –0.2 |
| | Stage II: Assimilation of mixed magma and intermediate lower crust (r = 0.36) | | | | | | | | | | |
| Mixed magma (F = 0.992) | 0.7071 | 392 | 1.5 | –3.5 | 21.1 | 0.1 | –0.8 | 4.0 | 0.1 | 5.8 | –0.1 |
| Upper crust | 0.7160 | 150 | 1.5 | –28.0 | 7.5 | 0.1 | –32.0 | 2.5 | 0.1 | –1.5 | –0.1 |

*Note:* Δ represents the difference in $\delta^{18}O$ between fractionating crystals and magma, i.e., $\Delta = \delta^{18}O$ (crystals) – $\delta^{18}O$ magma. WR—whole rock; Bulk D—bulk partition coefficient.

composition of the Eocene plutons now exposed to the surface may reflect the average composition of the potential lower crust reservoir. The Sr, Nd, O, and Hf isotopic composition of this potential lower crust reservoir was estimated to be $^{87}Sr/^{86}Sr_{10} = 0.7108$, $\varepsilon_{Nd_{(10)}} = -18$, $\delta^{18}O_{wr} = 7.1‰$, and $\varepsilon_{Hf_{(10)}} = -22$ based on values determined from the Eocene Emigrant Pass pluton (Table 2; Fig. 13; Konstantinou et al., 2013). This deep crustal reservoir has normal $\delta^{18}O_{wr} \approx 7.1‰$, similar to values calculated by analyzing zircon from the Eocene plutons (Table 2; Fig. 13B; Konstantinou et al., 2013). The normal $\delta^{18}O_{wr}$ of the lower crustal reservoir reflects the inability of meteoric fluids to infiltrate beneath the brittle-ductile transition zone (depths of ~10 km; Person et al., 2007) and shift the oxygen isotope composition of the deep crust to lower and/or negative values.

The geochemical compositions of possible asthenospheric or lithospheric mantle reservoirs that contributed melts to the lower crust during the Cenozoic is poorly constrained, primarily because of the extensive contamination of mantle-derived basalts by lower crustal melts. However, He isotope compositions from Miocene and Pleistocene basalts within the SRP indicate that these magmas may be mixtures between a mantle plume and a lithospheric mantle reservoir (Graham et al., 2009). For this study, we estimated that the unmodified isotopic composition of the Miocene mantle-derived basalts represented the mean composition of three end-

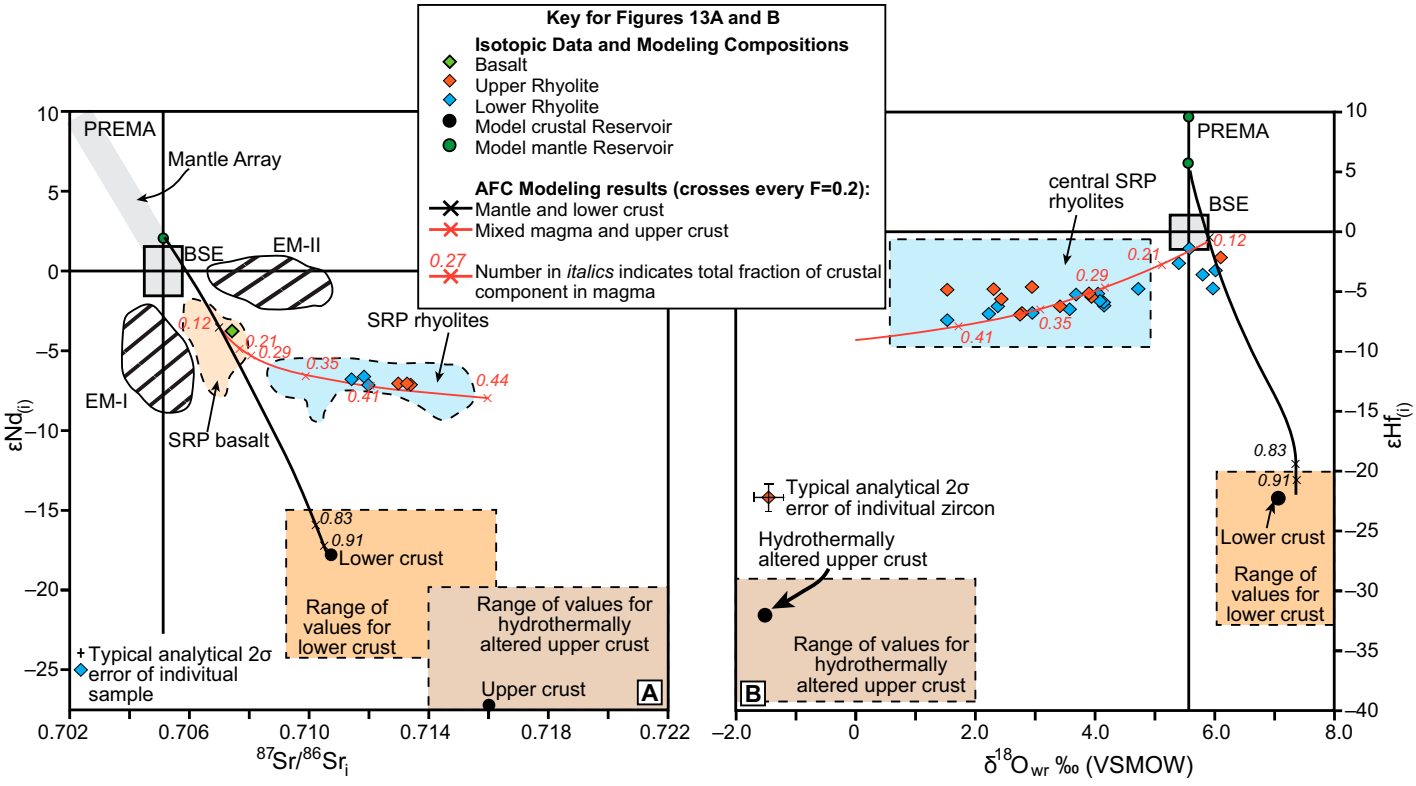


**Figure 13. (A) $^{87}Sr/^{86}Sr_i$ versus $\varepsilon_{Nd_{(i)}}$ compositions of samples from Jim Sage volcanic suite (JSVS), the basalt of Cotterel Mountains (Williams et al., 1982) and field of isotopic values from the central Snake River Plain (SRP) province. PREMA—prevalent mantle; EM-I—enriched mantle I; EM-II—enriched mantle II; BSE—bulk silicate earth. (B) $\delta^{18}O_{wr}$ (wr—whole rock; calculated from zircon $\delta^{18}O$) versus $\varepsilon_{Hf_{(i)}}$ compositions determined from individual zircon grains from samples of the JSVS, and field of isotopic values from the central SRP province. Results from AFC (assimilation–fractional crystallization) isotopic modeling show the relative crust versus mantle components represented by the Miocene magmas (see discussion in text and Table 2). Range of SRP isotopic values is from Christiansen and McCurry (2008), Watts et al. (2010), and Nash et al. (2006). VSMOW—Vienna standard mean ocean water.**

member mantle reservoirs, using the range of values summarized in Rollinson (1993). The three mantle reservoirs used were mantle plume and/or prevalent mantle, ancient enriched lithospheric mantle (lower $\varepsilon_{Nd}$, $\varepsilon_{Hf}$ than plume value), and a fluid-enriched (higher $^{87}Sr/^{86}Sr$ than plume value) lithospheric mantle (Fig. 13; Table 2; references in Rollinson, 1993).

## DISCUSSION

### Petrogenesis of the Jim Sage Volcanic Suite

The similarity of zircon $\varepsilon_{Hf_{(i)}}$ values measured from an exposed subvolcanic intrusion and the lava samples of the JSVS indicates that this (and possibly other) subvolcanic intrusion is part of the volcanic vent system for the eruption of the lavas of the JSVS (Fig. 12B). Thus, the occurrence of lava flows, lava domes, and subvolcanic intrusions within the Raft River Basin implies that the JSVS erupted within the basin, and the rhyolite lavas did not flow very far from their vents (<30 km). The northern part of the JSVS was capped by ignimbrite and basalt flows derived from the central SRP.

The age range of the rocks in the JSVS, together with their whole-rock major, trace element, and isotopic compositions and their zircon oxygen and Hf isotope compositions, are very similar to geochemical data sets collected on the high-temperature rhyolites from the central SRP (e.g., Bonnichsen and Citron, 1982; Honjo et al., 1992; Boroughs et al., 2005; Cathey et al., 2007, 2008; Branney et al., 2008; Christiansen and McCurry, 2008; Figs. 8, 11, and 12), suggesting that the JSVS is clearly a part of the SRP province. The high temperature of the rhyolite lavas (estimated from pyroxene compositions; Fig. 10) is consistent with a large flux of asthenosphere-derived basalt (hotspot) that in turn led to widespread crustal melting, as suggested for the magmas of the SRP province (e.g., Nash et al., 2006; McCurry and Rodgers, 2009).

### Isotopic Modeling of the Miocene Magmas of the JSVS and Central SRP

Our extensive isotopic data set from once deep-seated rocks of the Albion–Raft River–Grouse Creek metamorphic core complex allows us to use these rocks as proxies for the composition of the upper and lower crust in modeling measured compositions in Miocene volcanic rocks. To model and evaluate the relative roles and components of mantle versus crustal material in the Miocene magmas of the JSVS and the central SRP province, we used the isotopic constraints provided by the upper and lower crust reservoirs (see discussion of possible crustal and mantle sources for geochemical modeling), and the equations of simultaneous assimilation and fractional crystallization (AFC) derived by DePaolo (1981). We also used the equation for estimating the ratio of mass of assimilated crust versus initial mass of magma from Aitcheson and Forrest (1994). We simultaneously modeled the isotopic data (Sr, Nd, O, and Hf) together with the Sr, Nd, and Hf elemental compositions and tried a range of geologically reasonable values for the independent variables, using A:FC rates (r value in DePaolo, 1981) and bulk partition coefficients (the final values used are reported in Table 2). The final Sr-Nd-O-Hf isotopic compositions of hybrid magmas predicted from our AFC model are compared to measured whole-rock values ($^{87}Sr/^{86}Sr_i$-$\varepsilon_{Nd_{(i)}}$; Fig. 13A) and to the calculated $\delta^{18}O_{wr}$ and $\varepsilon_{Hf_{(i)}}$ based on measured isotopic values from Miocene zircon (calculated $\delta^{18}O_{wr}$ and $\varepsilon_{Hf_{(i)}}$; Fig. 13B).

We used a two-stage assimilation model for magma genesis (e.g., Gans et al., 1989; Grunder, 1993; Watts et al., 2010) that involves the high-temperature interaction of mantle-derived basalts with partial melts from the modeled normal $\delta^{18}O$ (≈7.0‰) lower crust reservoir (see discussion of possible crustal and mantle sources; Table 2) and high (r = 0.96) A:FC rates, approaching zone-refining values, shown by the black lines in Figures 13A and 13B. The high A:FC rates (r = 0.96) were chosen to reflect the high flux of basaltic melts that intruded the lower crust during the Miocene. Based on this modeling, we suggest that the basalt of the Cotterel Mountains and other basalts in the SRP may be contaminated with small amounts (~10%) of lower crust melts (Fig. 13), although the isotopic values for the basalt may also reflect contamination from a lithospheric mantle source.

This contaminated magma was further hybridized by variable amounts of partial melts from the modeled upper crust reservoir (red lines in Figs. 13A, 13B; isotopic values in Table 2), but at lower A:FC rates (r = 0.34). The upper crust assimilant has a negative $\delta^{18}O_{wr}$ ≈ –1.5‰, similar to values used in modeling of the SRP province (e.g., Watts et al., 2010, 2011). Our modeling suggests that the rhyolites of the JSVS and the SRP can be explained by the high-temperature interaction of crust-contaminated basalt (similar to the Cotterel basalt) followed by large amounts of assimilation of upper crust rocks. More specifically, our AFC modeling indicates that the Miocene rhyolites of the SRP may represent hybrid magmas composed of ~60% mantle-derived basalt, and ~40% crustal melts derived from two modeled crustal reservoirs; a normal $\delta^{18}O$ (≈7.1‰) lower crust, and a negative $\delta^{18}O$ (≈–1.5‰) hydrothermally altered upper crust reservoir (Fig. 13). The relatively low A:FC rates (r = 0.34) used in modeling the interaction of contaminated basalt with upper crustal rocks indicates high crystal fractionation rates, which were probably enhanced by the residence of rhyolitic magma chambers at shallow crustal levels (6–10 km). Based on regional stratigraphic studies in southern Idaho, the crust at 6–10 km may have been dominated by the presence of carbonate rocks (see discussion of possible crustal and mantle sources). However, depending on the extensional histories of the crust in this region, structurally deeper crystalline basement and overlying Neoproterozoic quartzites and schists may have been at shallower levels or 5–10 km deep (they are at the surface in the Albion–Raft River–Grouse Creek metamorphic core complex). Residence of rhyolitic magma chambers at shallow, relatively cool crustal levels (~5–10 km) has been documented today by the geophysical imaging of low-velocity zones interpreted to be shallow crystal-rich mushes beneath Yellowstone (e.g., Chu et al., 2010).

The low A:FC rates used to model the rhyolites of the SRP and the JSVS indicate that these low-silica rhyolite may have evolved by ~80% crystal fractionation (modeled at a partial melt fraction F = 0.2), coupled with assimilation (Fig. 8). Crystal fractionation helps to decrease the volume of the melt in the magmatic system undergoing AFC processes, thus producing low-$\delta^{18}O$ values with smaller amounts of crustal component than those predicted by simple mixing models. To illustrate this, we were able to successfully model rhyolite magma of $\delta^{18}O_{wr}$ ≈ 2.0‰ using the AFC model and assimilating ~30% crust with $\delta^{18}O_{wr}$ = –1.5‰ by ~70% of already contaminated (by 10% of crustal melts) basalt with $\delta^{18}O_{wr}$ = 5.8‰ (Fig. 13B). If a simple mixing model is used with the same crust-basalt end members ($\delta^{18}O_{wr}$ = –1.5‰ and 5.8‰ for crust and contaminated basalt, respectively), and crust to contaminated basalt mixing ratios of 30%:70%, the resulting $\delta^{18}O_{wr}$ would be ~3.6‰, and not ~2.0‰ predicted by the AFC model.

### Low-$\delta^{18}O$ Rhyolites of the JSVS

The low-$\delta^{18}O$ values of the JSVS rhyolite lavas that were erupted within the Raft River Basin, ~50 km south of the SRP province, require the assimilation of hydrothermally altered crust at shallow levels as proposed for the SRP rhyolites. However, there are no known long-lived caldera systems within the Raft River Basin, thus the low-$\delta^{18}O$ signature of the JSVS cannot be attributed to repeated caldera collapse events that drop hydrothermally altered rocks into the magmatic system (e.g., Bindeman and Valley, 2001; Bindeman et al., 2007; Watts et al.,

2011; Drew et al., 2013). We suggest two ways to explain the low-$\delta^{18}O$ signature of the JSVS lavas that erupted outside the SRP province. Each of these suggestions (model A and model B) (Fig. 14) has its strengths and limitations.

### *Model A: Low-$\delta^{18}O$ Silicic Melt Propagation Along a Preexisting Normal Fault*

The eruption of low-$\delta^{18}O$ rhyolites outside the main SRP province may be explained by the shallow-level (<10 km) propagation of hundreds of cubic kilometers of low-$\delta^{18}O$ rhyolite magma from the central SRP magma chambers to a magma chamber beneath the JSVS (Fig. 14; model A). The low-$\delta^{18}O$ signature of the rhyolite melt is produced within the SRP-Yellowstone province via one of the processes described herein (see discussion of Cenozoic extensional and magmatic history of the Basin and Range province; e.g., cf. Bindeman et al., 2007; Boroughs et al., 2005, 2012; Fig. 14; model A), and via AFC processes (as described in the discussion of isotopic modeling). This model is successful at explaining the similar compositions of all the isotopic systems (Sr-Nd-O-Hf) between the SRP and the JSVS, because the JSVS is essentially connected with the magmatic system of the central SRP at shallow depths (see the discussion of isotopic modeling). The propagation of the rhyolite beneath the Raft River Basin occurs along north-south conduits perhaps controlled by the geometry of the major north-south–trending normal fault (the Albion fault) that bounds the Albion Mountains on its eastern side. The Albion fault was an important Miocene crust-penetrating structure and possibly served as a structural weakness in the upper crust (Konstantinou et al., 2012; Konstantinou, 2013). Based on the extensional history of the Albion–Raft River–Grouse Creek metamorphic core complex (Konstantinou et al., 2012; Konstantinou, 2013), the elastic crust in the region of southern Idaho underwent high extensional strain rates from ca. 14 until after 8 Ma, and during that time major SRP magma chambers may have been just north of the Albion–Raft River–Grouse Creek metamorphic core complex. This magma chambers may have acted as large heterogeneous bodies in the elastic crust having completely different physical properties (e.g., viscosity, stiffness) relative to the extending elastic crust. This less stiff inclusion may have focused the extensional strain in the elastic crust along the northern and southern tips around the magma chamber and may have assisted in the propagation of rhyolitic melt along north-south–trending avenues in the shallow crust. This process may be analogous (at a different scale) to borehole wall breakouts, which form symmetrically at the orientation of least principal horizontal stress, due to the concentration of stress around the borehole.

The major pitfall of this model of explaining the JSVS is achieving the physical propagation of rhyolite melt within the crust, over large distances (~50 km; Fig. 14; model A). This is problematic due to the high viscosity of silicic melt that would cause them to quench during injection over large distances. Few studies have focused on silicic melt propagation along structures in the upper crust, but an example may be the 222–196 Ma, 18 km linear trend of a silicic dike swarm in the Candelaria mining district in western Nevada (Thomson et al., 1995). Lateral migration of silicic magma along faults in the Aso Caldera, southwestern Japan has also been demonstrated (Miyoshi et al., 2013). Another problematic aspect of this model is that large amounts of hydrothermally altered rocks with negative $\delta^{18}O$ are required to produce the large-volume magmas of the SRP (and the JSVS; see the discussion of isotopic modeling). These extremely low $\delta^{18}O$ rocks are rare in the geologic record of the region, but we envision that some of these rocks are faulted and buried beneath younger volcanic rocks within the SRP, and thus inaccessible for study.

### *Model B: Large-Scale Crustal Melting Beneath the Raft River Basin*

An alternative explanation for the occurrence of the low-$\delta^{18}O$ rhyolite lavas of the JSVS (Fig. 14; model B) might entail melting of hydrothermally altered crust outside the SRP-Yellowstone province and directly beneath the Raft River Basin. We envision that a normal $\delta^{18}O$ (≈5.6‰) basaltic plumbing system of the JSVS may have been connected to that of the SRP-Yellowstone province at deeper levels, either within the lower crust or at the base of the crust (Fig. 14; model B). In model B, the low-$\delta^{18}O$ rhyolite magmas of the JSVS may have formed by the interaction of a large flux of basalt with hydrothermally altered crust at depths of 6–8 km beneath the Raft River Basin, resulting in large-scale crustal melting but not significant mixing and/or assimilation of these crustal melts with the basalt (Fig. 14). Melting of the crust on an extensive scale (rather than AFC processes; see the discussion of isotopic modeling) would require a smaller volume (~500 km$^3$) of low-$\delta^{18}O_{wr}$ upper crust, with $\delta^{18}O_{wr}$ of ~2.5‰ to produce the rhyolites of the JSVS.

Because rocks with $\delta^{18}O_{wr}$ of 2‰–3‰ are more common in the region (e.g., Criss and Taylor, 1983; Criss et al., 1984; <200 km north of the Raft River Basin), both the $\delta^{18}O_{wr}$ ≈ 2.5‰ and the volume of the hydrothermally altered crust are not as problematic as the values required for modeling the rhyolites of the SRP province ($\delta^{18}O_{wr}$ ≈ –1.5‰; see the discussion of isotopic modeling).

Because there are no known caldera complexes in the Raft River Basin to explain the hydrothermal alteration of the crust, we propose alternative mechanisms for the formation of ~500 km$^3$ of low-$\delta^{18}O$ crust beneath the Raft River Basin. Measured zircon $\delta^{18}O$ values for deep Archean–Oligocene crustal rocks in the Albion–Raft River–Grouse Creek metamorphic core complex indicate that they have normal magmatic $\delta^{18}O_{wr}$ values ($\delta^{18}O_{wr}$ ≈ 7.1‰; see discussion of possible crustal and mantle sources; Strickland et al., 2011b; Konstantinou et al., 2013). These relationships imply that the alteration was synchronous, or younger than Oligocene, and a plausible mechanism for the hydrothermal alteration of the upper crust may be related to extensional deformation during the formation and localized rise of metamorphic core complexes. Oligocene granite-cored gneiss domes first rose diapirically to the base of the upper crust over a protracted period of time (32–25 Ma; Fig. 14; Strickland et al., 2011a, 2011b; Konstantinou et al., 2012). The regions around and between the granite-core gneiss domes may have been intensely faulted and fractured (see discussion in Konstantinou et al., 2012, and numerical modeling by Rey et al., 2011). These fractures would have brecciated large volumes of the Archean basement and the Proterozoic schist units above and away from the gneiss domes. A large number of closely spaced faults may have potentially provided multiple conduits for meteoric fluids to percolate at depths of 6–10 km. The emplacement of the Oligocene plutons and the rise of the hot crust of the gneiss domes may have provided the necessary heat to exchange oxygen between low-$\delta^{18}O$ meteoric fluids and the Archean basement, and Proterozoic metapelites thus may have resulted in the formation of a low-$\delta^{18}O$ crustal reservoir in the brecciated and metamorphosed region between and around the gneiss domes.

Oxygen isotope studies of rocks within and around other metamorphic core complexes in the western U.S. indicate that low-$\delta^{18}O$ zones are common in the brecciated and chloritized regions around the complexes. For example, in the Valhalla gneiss dome, 1–2-km-thick upper plate chloritic breccias have $\delta^{18}O_{wr}$ and $\delta^{18}O_{feld}$ (feld—feldspar) that range from ~5‰ to –5‰, even though the mylonite zones $\delta^{18}O_{wr}$ and $\delta^{18}O_{feld}$ values that range from 11‰ to 2‰ (Holk and Taylor, 2007). Another example is the Bitterroot metamorphic core complex, where chloritic breccias above the mylonite zones have $\delta^{18}O_{wr}$ and $\delta^{18}O_{feld}$ that range from ~6‰ to –4‰, and the mylonite zones have $\delta^{18}O_{wr}$ and $\delta^{18}O_{feld}$ values that range from 12‰ to –1‰

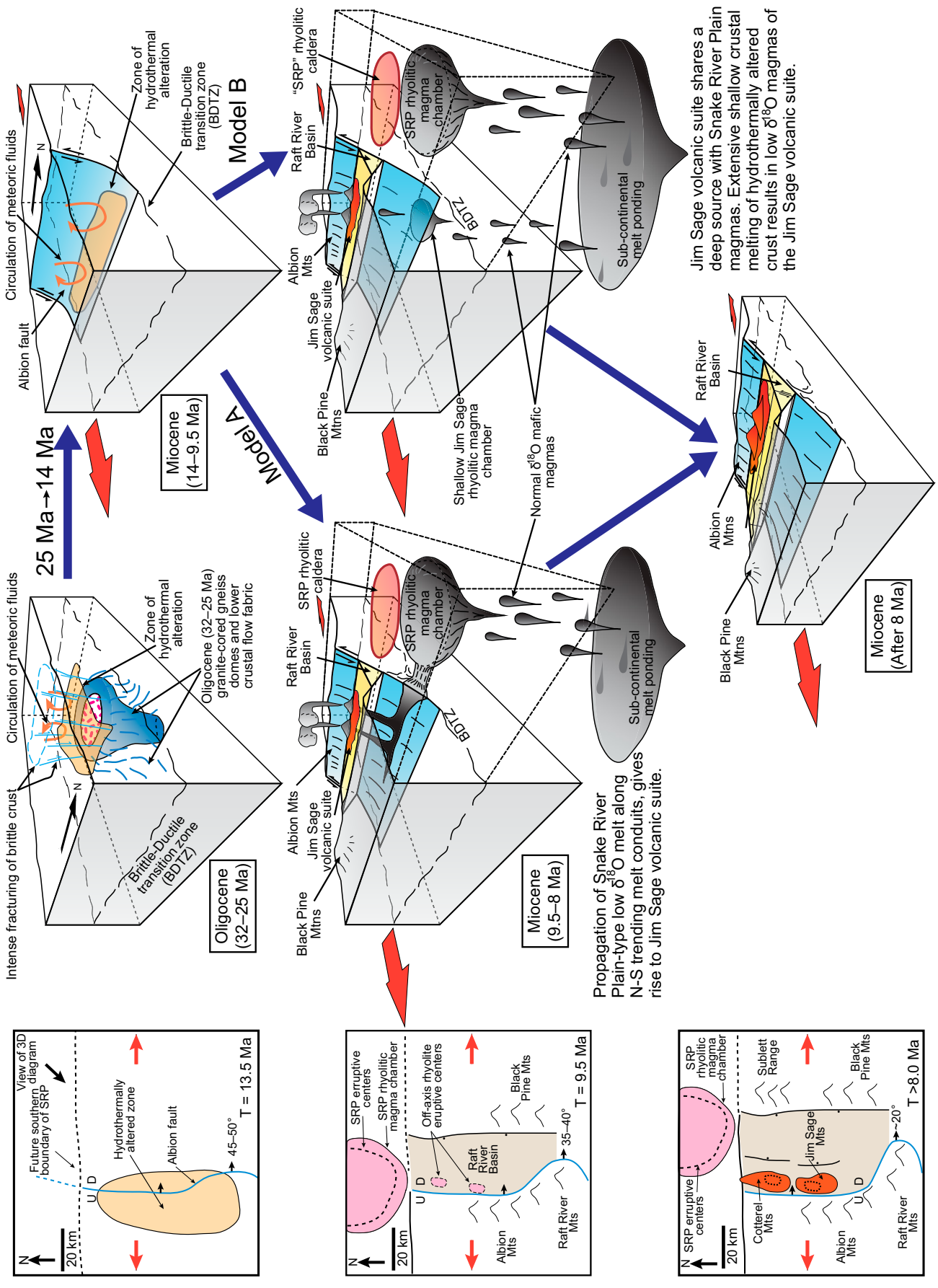


**Figure 14. Summaries of the two models proposed to explain the emplacement of the Jim Sage volcanic suite (JSVS) and its relationship to the Snake River Plain province (SRP) and motion along the Albion fault. Note that the view for the diagrams is from the north (SRP) looking south. U—upthrown; D—downthrown; Mts—Mountains; BDTZ—Brittle-ductile transition zone.**

(Kerrich and Hyndman, 1986). In the Albion–Raft River–Grouse Creek metamorphic core complex, retrogression of garnet and staurolite to white mica and chlorite away from the Oligocene gneiss domes is widespread in the Precambrian schist units. This retrogression affects much larger volumes of crust than those that are metamorphosed to sillimanite-grade rocks in the carapaces of the actual gneiss domes. However, there has been no systematic study of the $\delta^{18}O$ values of these rocks, but such a study might offer insight into the $\delta^{18}O_{wr}$ composition of the crust in this region.

Another way of possibly forming a low-$\delta^{18}O$ crustal reservoir is via the percolation of meteoric fluids deep into the crust along the Miocene Albion fault system (Konstantinou et al., 2012), when large volumes of meteoric fluids may have percolated to ~8 km and exchanged oxygen with the silicic rocks of the Archean basement, the Proterozoic schist units, or Cenozoic granites, thus forming a localized low-$\delta^{18}O$ reservoir. Providing support for fault-related hydrothermal circulation systems are recent studies of ductilely deformed rocks in the Raft River detachment that, based on their hydrogen isotopes, show evidence of percolation of meteoric fluids at deep crustal levels that are now exposed to the surface (Gottardi et al., 2011). These studies show that normal fault systems provide the necessary conduits for meteoric fluids to circulate to depths of 10 km in the crust, to the brittle-ductile transition zone.

Model B portrayed in Figure 14 has a major limitation. If the JSVS represents large-scale crustal melting of rocks similar to the Archean basement, the Proterozoic schist units and the Oligocene granites exposed today in the adjacent metamorphic core complex, then the Sr-Nd-Hf isotope compositions of the JSVS should be nearly identical to the compositions of rocks exposed in the complex. However, the rhyolites of the JSVS have much less evolved Sr-Nd-Hf compositions than the compositions represented by the silicic rocks within the Albion–Raft River–Grouse Creek metamorphic core complex (e.g., Strickland et al., 2011b; Konstantinou et al., 2013; Fig. 13). Thus model B may not effectively predict all the measured isotopic compositions of the magmas at the JSVS.

### Implications for the Evolution of the Raft River Detachment and Basin and Range Faulting

The eruption of ~240 $km^3$ of high-temperature rhyolite in the synextensional Raft River Basin has important implications for the evolution of Basin and Range faulting and the exhumation of the adjacent Albion–Raft River–Grouse Creek metamorphic core complex. The data (and preceding discussion) establish a direct link between magmatism in the JSVS and the central SRP-Yellowstone province based on similar timing, geochemistry, and isotopic compositions. The data might also imply that a silicic Miocene pluton with possible mafic roots could directly underlie the Raft River Basin (Fig. 14; model B). This inferred high-level Miocene silicic magmatic system would, as for the SRP, be driven by a high flux of basalt and thermal input to the middle and lower crust of southern Idaho and may have led to extensive crustal melting at shallow levels of the crust beneath the region of the Raft River Basin and the Albion–Raft River–Grouse Creek metamorphic core complex. The structural history of the Raft River Basin (as detailed by Konstantinou et al., 2012; Konstantinou, 2013) indicates that the rotation of the Albion fault to shallow angles and all of the normal faulting and rotation of Miocene basin fill strata occurred after the eruption of the JSVS (after 8.2 Ma; Konstantinou et al., 2012). This young faulting and extension is most easily explained by coeval doming with a component of vertical uplift during horizontal stretching of the crust beneath the Raft River Basin. Horizontal extension and vertical uplift resulted in the present-day subhorizontal geometry of the basal detachment imaged seismically beneath the Raft River Basin (Covington, 1983; Konstantinou et al., 2012; Konstantinou 2013).

The possible existence at depth of a silicic magmatic system implies (as it does for the SRP-Yellowstone) addition of basaltic material at greater depth in the crust and concomitant heating of the middle and lower crust leading to possibly extensive crustal melting beneath the region of the Albion–Raft River–Grouse Creek metamorphic core complex during the Miocene. This crustal melting event may have resulted in increased mobility of the deep crust during and after the eruption of the rhyolite lavas. We therefore interpret the extensional deformation and vertical component of uplift after ca.8.2 Ma to be a direct consequence of greater mobility of the immediately underlying crust.

## CONCLUSIONS

The JSVS is composed of ~240 $km^3$ of rhyolite lavas, capped by central SRP–derived rheomorphic ignimbrites and a thin sequence (<100 m) of Miocene basalt flows. The rhyolite lavas of the JSVS erupted from small centers within the Raft River Basin based on their physical attributes (aspect ratios and basal contact) and the occurrence of subvolcanic intrusions and domes. The ignimbrite and basalts are probably outflows from the central SRP. The major and trace element and isotopic compositions of the rhyolite lavas are consistent with having an origin similar to that of the magmas in the central SRP-Yellowstone province. This observation, coupled with the fact that the rhyolites have a low-$\delta^{18}O$ signature, suggests that the in situ assimilation of hydrothermally altered caldera blocks proposed to explain the origin of low-$\delta^{18}O$ rhyolites in the SRP may not have been the case here. We offer two models that might explain the low-$\delta^{18}O$ signature of the lavas in the JSVS, each with their own strengths and limitations. The first model suggests that SRP-type rhyolitic melt propagated southward along the Albion fault to erupt in the center of the Raft River Basin. The second model proposes that the hydrothermal alteration of the crust in the region of southern Idaho may be more widespread than previously thought and was related to the earlier igneous and gneiss dome history or the normal faulting history of the region, and that the eruption of the JSVS was localized above a magma chamber off axis of the SRP. It is possible that a low-$\delta^{18}O$ silicic pluton beneath the Raft River Basin could have provided a heat source for crustal melting and weakening that led to extension accompanied by vertical doming and rise of the Raft River Basin after the eruption of the JSVS rhyolites.

### ACKNOWLEDGMENTS

We thank Stanford University for the Stanford Graduate Fellowship that supported this research for three years, ExxonMobil for a science grant, and the Leventis Foundation and the Stanford McGee Funds for providing financial support for the analytical part of this project. Support was also provided by the National Science Foundation (NSF) Tectonics Division (grants EAR-0809226 and EAR-0948679 to Miller). Gail Mahood, Matt Coble, and Eric Gottlieb provided helpful discussions and insights about the scientific work presented herein. Mike McCurry, Ilya Bindeman, and Ben Ellis provided valuable reviews that greatly improved the paper. We thank Noriko Kita and Kouki Kitajima for assistance with secondary ion mass spectrometer (SIMS) analysis of oxygen isotope ratios. The University of Wisconsin WiscSIMS is partially supported by NSF grants EAR-0319230, EAR-0744079, and EAR-1053466. The Washington State University Radiogenic Isotope and Geochronology Laboratory is partially supported by NSF grants EAR-0844149, EAR-1019877, and EAR-1119237. We thank Karrie Weaver and Caroline Harris for their help with the whole-rock Sr and Nd isotope analyses.

### APPENDIX 1. METHODS FOR WHOLE-ROCK TRACER ISOTOPE ANALYSES

Samples were selected and processed at the Stanford University ICP-MS-TIMS (inductively coupled plasma–mass spectrometry–thermal ionization mass spectrometry) facility. The samples were chipped, and rock chips were hand-selected and pulverized to a very fine powder using an agate shutter box bowl. A small aliquot of each sample (40–60 mg) was dissolved in Savillex Teflon vials using a combination of 29 N HF,

followed by a mixture of 3:1 ratio of 10.5 N HCl and 14 N $HNO_3$. An aliquot of the solution was dried and the salt was redissolved in HCl to prepare for column chromatography. Strontium and the rare earth elements (REE) were separated from major elements and other trace elements using an HCl elution on 200–400 mesh AG50-X8 cation exchange resin. The Sr was further isolated from Rb using Eichrom 20–50 µm Sr-spec resin in Teflon microcolumns. Elemental Nd was purified from the REE aliquot of the cation exchange column by column chromatography using Eichrom 50–100 µm LN-spec resin. The chemistry was monitored to ensure adequate separation of Nd from Ce and Sm, the isobaric interferences of which may compromise the quality of the isotopic analyses. The resulting purified Sr and Nd salts were prepared for mass spectrometry analysis by redissolving them in 2% $HNO_3$. Isotope analyses were performed using the Nu-Instruments Plasma HR multicollector ICP-MS.

Each Sr isotope analysis consisted of 50 cycles of 10 s integration time, split into 2 blocks, during which 6 isotopes were measured simultaneously ($^{83}$Sr, $^{84}$Kr, $^{84}$Sr, $^{85}$Rb, $^{86}$Sr, $^{87}$Sr, $^{88}$Sr) on Faraday cups. Instrumental mass fractionation and $^{86}$Kr interference on $^{86}$Sr were corrected for by subtracting the $^{84}$Kr to obtain the natural $^{84}$Sr/$^{88}$Sr ratio of 0.00675476 while iteratively solving for the exponential fractionation factor and Kr correction on $^{86}$Sr, an approach similar to that of Jackson and Hart (2006). Baselines were measured at 0.25 amu from peak center to account for scattering of $^{40}Ar_2$ that creates a nonlinear baseline across the Sr masses. Interference on $^{87}$Sr from $^{87}$Rb was small and corrected using $^{85}$Rb and the instrumental mass fractionation factor for Sr; 43 analyses of SRM 987 resulted in an average $^{87}$Sr/$^{86}$Sr value of 0.710144 ± 52 (2σ). Sample ratios were multiplied by a normalization factor determined by correcting SRM 987 analyses to a value of $^{87}$Sr/$^{86}$Sr = 0.71025 ± 1 (2σ; Balcaen et al., 2005) and the external error based on the 31 SRM 987 analyses was added to the analytical error for each sample. The total mass of sample analyzed ranged from 20 to 50 ng, and a blank analysis yielded an estimated mass of Sr < 0.01 ng. A secondary standard of BHVO-1 was analyzed 7 times and yielded an average value of 0.703483 ± 14 (2σ) [accepted value is 0.703475 ± 17 (2σ); Weiss et al., 2005] after correction using the normalization factor obtained from SRM 987.

Each Nd isotope analysis consisted of 40 cycles of 10 s integration time, split into 2 blocks, during which 5 isotopes were measured simultaneously ($^{143}$Nd, $^{144}$Nd, $^{145}$Nd, $^{146}$Nd, and $^{144}$Sm), monitored for Ce and Sm interferences. Mass bias was exponentially corrected based on a $^{146}$Nd/$^{144}$Nd ratio of 0.7219. Sample ratios were multiplied by a normalization factor determined from 26 analyses of JNdi-1 resulted in an average $^{143}$Nd/$^{144}$Nd value of 0.512087 ± 22 (2σ). The total mass of sample analyzed ranged from 10 to 30 ng, and a blank analysis yielded an estimated mass of Nd < 0.005 ng. A secondary standard of BHVO-1 was analyzed 3 times and yielded an average value of $^{143}$Nd/$^{144}$Nd 0.512969 ± 20 (2σ). This compares to the value for BHVO-1 of $^{143}$Nd/$^{144}$Nd = 0.512986 ± 18 (2σ) from Weiss et al. (2005).

## APPENDIX 2. METHODS FOR OXYGEN ISOTOPE ANALYSES

Oxygen isotope analysis was performed at the University of Wisconsin WiscSIMS (Wisconsin Secondary Ion Mass Spectrometer) laboratory using a CAMECA IMS-1280 ion microprobe following the procedures outlined in Kita et al. (2009) and Valley and Kita (2009). The zircon crystals were mounted with the KIM-5 O isotope standard (Valley, 2003; $\delta^{18}O$ = 5.09‰ Vienna standard mean ocean water, VSMOW), and polished prior to O isotope analyses. Extra care was taken to achieve a smooth, flat, low-relief polish. An ~2 nA primary beam of $^{133}Cs^+$ was focused to 10-µm-diameter spots on the sample. A normal-incidence electron gun and carbon coat were used for charge compensation. The secondary ion acceleration voltage was set at 10 kV and the O isotopes were collected in 2 Faraday cups simultaneously in multicollection mode. Four consecutive measurements on KIM-5 zircon standard ($\delta^{18}O$ = 5.09‰ VSMOW; Valley, 2003) were analyzed before and after groups of 10–20 sample spots. The 2 SD precision for bracketing groups of eight standard analyses is reported as external precision for sample data. The average values of the standard analyses that bracket each set of unknowns were used to correct for instrumental bias. The average precision (reproducibility) of the bracketing standards for this study ranged from ±0.13 to ±0.35 and averaged ±0.26‰ (2 SD). After O isotope analysis, ion microprobe pits were imaged by secondary electron microscopy and pits that were located on obvious cracks or inclusions were excluded from the data set.

## APPENDIX 3. METHODS FOR HAFNIUM ISOTOPE ANALYSES

Hf isotopic compositions were determined on zircons from five Miocene samples at Washington State University's LA-MC-ICP-MS (laser ablation–multicollector–inductively coupled plasma–mass spectrometry) facility, using the procedure from C.M Fisher (2013, personal commun.). The resulting isotopic ratios were evaluated based on the quality and duration of the Hf analysis; 40 zircon Hf isotope analyses yielded $^{176}$Hf/$^{177}$Hf ratios that were corrected for interlaboratory bias using the R33 standards (correction factor = 1.000159), and the corrected ratios, along with measured $^{176}$Lu/$^{177}$Hf and sensitive high-resolution ion microprobe–reverse geometry ages, were used to calculate $\varepsilon_{Hf_{(i)}}$ and $\varepsilon_{Hf_{(t)}}$ values. The results are reported in Supplemental Table 6 (see footnote 6). Isotopic ratios with values ranging from $\varepsilon_{Hf_{(t)}}$ –25 to –44 were excluded from further consideration (n = 8) because they could represent mixed isotopic compositions resulting from ablation and analysis of Miocene magmatic zircon and inherited zircon cores.

## REFERENCES CITED


Aitcheson, S.J., and Forrest, A.H., 1994, Quantification of crustal contamination in open magmatic systems: Journal of Petrology, v. 35, p. 461–488, doi:10.1093/petrology/35.2.461.

Anders, M.H., and Sleep, N.H., 1992, Magmatism and extension; the thermal and mechanical effects of the Yellowstone hotspot: Journal of Geophysical Research, v. 97, no. B11, p. 15379–15393, doi:10.1029/92JB01376.

Andrews, G.D.M., and Branney, M.J., 2011, Emplacement and rheomorphic deformation of a large, lava-like rhyolitic ignimbrite: Grey's landing, southern Idaho: Geological Society of America Bulletin, v. 123, p. 725–743, doi:10.1130/B30167.1.

Andrews, G.D.M., Branney, M.J., Bonnichsen, B., and McCurry, M., 2008, Rhyolitic ignimbrites in the Rogerson Graben, southern Snake River Plain volcanic province: Volcanic stratigraphy, eruption history and basin evolution: Bulletin of Volcanology, v. 70, p. 269–291, doi:10.1007/s00445-007-0139-0.

Armstrong, R.L., Leeman, W.P., and Malde, H.E., 1975, K-Ar dating, Quaternary and Neogene volcanic rocks of the Snake River plain, Idaho: American Journal of Science, v. 275, p. 225–251, doi:10.2475/ajs.275.3.225.

Balcaen, L., De Schrijver, I., Moens, L., and Vanhaecke, F., 2005, Determination of the $^{87}$Sr/$^{86}$Sr isotope ratio in USGS silicate reference materials by multi-collector ICP–mass spectrometry: International Journal of Mass Spectrometry, v. 242, p. 251–255, doi:10.1016/j.ijms.2004.10.025.

Barth, A.P., and Wooden, J.L., 2010, Coupled elemental and isotopic analyses of polygenetic zircons from granitic rocks by ion microprobe, with implications for melt evolution and the sources of granitic magmas: Chemical Geology, v. 277, p. 149–159, doi:10.1016/j.chemgeo.2010.07.017.

Best, M.G., and Christiansen, E.H., 1991, Limited extension during peak tertiary volcanism, Great Basin of Nevada and Utah: Journal of Geophysical Research, v. 96, no. B8, p. 13509–13528, doi:10.1029/91JB00244.

Bindeman, I.N., and Valley, J.W., 2001, Low-delta $^{18}$O rhyolites from Yellowstone: Magmatic evolution based on analyses of zircons and individual phenocrysts: Journal of Petrology, v. 42, p. 1491–1517, doi:10.1093/petrology/42.8.1491.

Bindeman, I.N., Valley, J.W., Wooden, J.L., and Persing, H.M., 2001, Post-caldera volcanism: In situ measurement of U-Pb age and oxygen isotope ratio in Pleistocene zircons from Yellowstone caldera: Earth and Planetary Science Letters, v. 189, p. 197–206, doi:10.1016/S0012-821X(01)00358-2.

Bindeman, I.N., Watts, K.E., Schmitt, A.K., Morgan, L.A., and Shanks, P.W.C., 2007, Voluminous low delta $^{18}$O magmas in the late Miocene Heise volcanic field, Idaho: Implications for the fate of Yellowstone hotspot calderas: Geology, v. 35, p. 1019–1022, doi:10.1130/G24141A.1.

Bindeman, I.N., Fu, B., Kita, N.T., and Valley, J.W., 2008, Origin and evolution of silicic magmatism at Yellowstone based on ion microprobe analysis of isotopically zoned zircons: Journal of Petrology, v. 49, p. 163–193, doi:10.1093/petrology/egm075.

Black, L.P., and 10 others, 2004, Improved $^{206}$Pb/$^{238}$U microprobe geochronology by the monitoring of a trace-element-related matrix effect: SHRIMP, ID-TIMS, ELA-ICP-MS, and oxygen isotope documentation for a series of zircon standards: Chemical Geology, v. 205, p. 115–140, doi:10.1016/j.chemgeo.2004.01.003.

Bonnichsen, B., and Citron, G.P., 1982, The Cougar Point Tuff, southwestern Idaho and vicinity, *in* Bonnichsen, B., and Breckenridge, R.M., eds., Cenozoic geology of Idaho: Idaho Bureau of Mines Geology Bulletin 26, p. 255–281.

Bonnichsen, B., Leeman, W.P., Honjo, N., McIntosh, W.C., Godchaux, M.M., McCurry, M., and Christiansen, E.H., 2008, Miocene silicic volcanism in southwestern Idaho: Geochronology, geochemistry, and evolution of the central Snake River plain: Bulletin of Volcanology, v. 70, p. 315–342, doi:10.1007/s00445-007-0141-6.

Boroughs, S., Wolff, J., Bonnichsen, B., Godchaux, M.M., and Larson, P., 2005, Large-volume, low-$\delta^{18}$O rhyolites of the central Snake River plain, Idaho, USA: Geology, v. 33, p. 821–824, doi:10.1130/G21723.1.

Boroughs, S., Wolff, J.A., Ellis, B.S., Bonnichsen, B., and Larson, P.B., 2012, Evaluation of models for the origin of Miocene low-$\delta^{18}$O rhyolites of the Yellowstone/Columbia River Large Igneous Province: Earth and Planetary Science. v. 313, p. 45–55, doi:10.1016/j.epsl.2011.10.039.

Bouvier, A., Vervoort, J.D., and Patchett, P.J., 2008, The Lu-Hf and Sm-Nd isotopic composition of CHUR: Constraints from unequilibrated chondrites and implications for the bulk composition of terrestrial planets: Earth and Planetary Science Letters, v. 273, p. 48–57, doi:10.1016/j.epsl.2008.06.010.

Boynton, W.V., 1985, Chapter 3: Cosmochemistry of the rare earth elements: Meteorite studies, *in* Henderson, P., ed., Rare Earth Element Geochemistry (Developments in Geochemistry 2): Amsterdam, Elsevier, p. 115–152.

Branney, M.J., Bonnichsen, B., Andrews, G.D.M., Ellis, B., Barry, T.L., McCurry, M., Christiansen, E.H., and Leeman, W.P., 2008, 'Snake River (SR)-type' volcanism at the Yellowstone hotspot track: Distinctive products from unusual, high-temperature silicic super-eruptions: Bulletin of Volcanology, v. 70, p. 293–314, doi:10.1007/s00445-007-0140-7.

Bryan, S.E., 2007, Silicic large igneous provinces: Episodes, v. 30, p. 20–31.

Bryan, S.E., Riley, T.R., Jerram, D.A., Stephens, C.J., and Leat, P.T., 2002, Silicic volcanism: An undervalued component of large igneous provinces and volcanic rifted margins, *in* Menzies, M.A., et al., eds., Volcanic rifted margins: Geological Society of America Special Paper 362, p. 97–118, doi:10.1130/0-8137-2362-0.97.

Burchfiel, B.C., Lipman, P.W., and Zoback, M.L.C., eds., 1992, The Cordilleran orogen: Conterminous U.S.: Boulder, Colorado, Geological Society of America, Geology of North America, v. G-3, 732 p.

Cathey, H.E., and Nash, B.P., 2009, Pyroxene thermometry of rhyolite lavas of the Bruneau–Jarbidge eruptive center, Central Snake River Plain: Journal of Volcanology and Geothermal Research v. 188, p. 173–185, doi:10.1016/j.jvolgeores.2009.05.024.

Cathey, H.E., Nash, B.P., Valley, J.W., Kita, N.T., Ushikubo, T., and Spicuzza, M.J., 2007, Pervasive and persistent large-volume, low $\delta^{18}O$ silicic magma generation at the Yellowstone hotspot: 12.7–10.5 Ma: Ion microprobe analysis of zircons in the Cougar Point tuff: Eos (Transactions, American Geophysical Union), v. 88, fall meeting supplement, abs.V51C–0708.

Cathey, H.E., Nash, B.P., Valley, J.W., Kita, N.T., Allen, C.M., and Campbell, I.H., 2011, A new model for large-volume low $\delta^{18}O$ silicic magmatism? Insights from zircons of the Cougar Point Tuff: Geological Society of America Abstracts with Programs, v. 44, no. 5, p. 652.

Christiansen, E.H., and McCurry, M., 2008, Contrasting origins of Cenozoic silicic volcanic rocks from the western cordillera of the United States: Bulletin of Volcanology, v. 70, p. 251–267, doi:10.1007/s00445-007-0138-1.

Christiansen, R.L., 2001, The Quaternary and Pliocene Yellowstone plateau volcanic field of Wyoming, Idaho, and Montana: U.S. Geological Survey Professional Paper 729-G, 120 p.

Christiansen, R.L., and Lipman, P.W., 1972, Cenozoic volcanism and plate-tectonic evolution of the western United States: II, Late Cenozoic: Royal Society of London Philosophical Transactions, ser. A, v. 271, p. 249–284, doi:10.1098/rsta.1972.0009.

Christiansen, R.L., and Yeats, R.S., 1992, Post-Laramide geology of the U.S. Cordilleran region, *in* Burchfiel, B.C., et al., eds., The Cordilleran orogen: Conterminous U.S.: Boulder, Colorado, Geological Society of America, Geology of North America, v. G-3, p. 261–406.

Chu, R., Helmberger D.V., Sun, D., Jackson, J.M., and Zhu, L., 2010, Mushy magma beneath Yellowstone: Geophysical Research Letters, v. 37, doi:10.1029/2009GL041656.

Coble, M.A., and Mahood, G.A., 2012, Initial impingement of the Yellowstone plume located by widespread silicic volcanism contemporaneous with Columbia River flood basalts: Geology, v. 40, p. 655–658, doi:10.1130/G32692.1.

Colgan, J.P., and Henry, C.D., 2009, Rapid middle Miocene collapse of the Mesozoic orogenic plateau in north-central Nevada: International Geology Review, v. 51, p. 920–961, doi:10.1080/00206810903056731.

Colgan, J.P., Dumitru, T.A., McWilliams, M., and Miller, E.L., 2006a, Timing of Cenozoic volcanism and Basin and Range extension in northwestern Nevada: New constraints from the northern Pine Forest Range: GSA Bulletin, v. 118, p. 126–139, doi:10.1130/B25681.1.

Colgan, J.P., Dumitru, T.A., Reiners, P.W., Wooden, J.L., and Miller, E.L., 2006b, Cenozoic tectonic evolution of the Basin and Range province in northwestern Nevada: American Journal of Science, v. 306, p. 616–654, doi:10.2475/08.2006.02.

Colgan, J.P., Shuster, D.L., and Reiners, P.W., 2008, Two-phase Neogene extension in the northwestern Basin and Range recorded in a single thermochronology sample: Geology, v. 36, p. 631–634, doi:10.1130/G24897A.1.

Colgan, J.P., Howard, K.A., Fleck, R.J., and Wooden, J.L., 2010, Rapid middle Miocene extension and unroofing of the southern Ruby Mountains, Nevada: Tectonics, v. 29, doi:10.1029/2009TC002655.

Compton, R.R., 1972, Geologic map of the Yost quadrangle, Box Elder County, Utah, and Cassia County, Idaho: U.S. Geological Survey Miscellaneous Geologic Investigations Map I-672, scale 1:31,680.

Compton, R.R., 1975, Geologic map of the Park Valley quadrangle, Box Elder County, Utah and Cassia County, Idaho: U.S. Geological Survey Miscellaneous Geologic Investigations Map I-873, scale 1:31,680.

Compton, R.R., Todd, V.R., Zartman, R.E., and Naeser, C.W., 1977, Oligocene and Miocene metamorphism, folding, and low-angle faulting in northwestern Utah: Geological Society of America Bulletin, v. 88, p. 1237–1250, doi:10.1130/0016-7606(1977)88<1237:OAMMFA>2.0.CO;2.

Covington, H.R., 1983, Structural evolution of the Raft River Basin, Idaho, *in* Miller, D.M., et al., eds., Tectonic and stratigraphic studies in the eastern Great Basin: Geological Society of America Memoir 157, p. 229–238, doi:10.1130/MEM157-p229.

Criss, R.E., and Taylor, H.R., Jr., 1983, An $^{18}O/^{16}O$ and D/H study of Tertiary hydrothermal systems in the southern half of the Idaho batholith: Geological Society of America Bulletin, v. 94, p. 640–663, doi:10.1130/0016-7606(1983)94<640:AOADSO>2.0.CO;2.

Criss, R.E., Erken, E.B., and Hardyman, R.F., 1984, Casto Ring Zone: A 4,500-km$^2$ fossil hydrothermal system in the Challis Volcanic Field, central Idaho: Geology, v. 12, p. 331–334, doi:10.1130/0091-7613(1984)12<331:CRZAKF>2.0.CO;2.

DeCelles, P.G., Lawton, T.F., and Mitra, G., 1995, Thrust timing, growth of structural culminations, and synorogenic sedimentation in the type Sevier orogenic belt, western United States: Geology, v. 23, p. 699–702, doi:10.1130/0091-7613(1995)023<0699:TTGOSC>2.3.CO;2.

DePaolo, D.J., 1981, Trace element and isotopic effects of combined wallrock assimilation and fractional crystallization: Earth and Planetary Science Letters, v. 53, p. 189–202, doi:10.1016/0012-821X(81)90153-9.

Drew, D., Bindeman, I., Watts, K., Schmitt, A., Fu, B., and McCurry, M., 2013, Crustal scale recycling in caldera complexes and rift zones of the Snake River Plain: O and Hf isotopic evidence in diverse zircons from low-$\delta^{18}O$ rhyolites of the Picabo volcanic field, Idaho: Earth and Planetary Science Letters (in press)

Egger, A.E., Dumitru, T.A., Miller, E.L., Savage, C.F.I., and Wooden, J.L., 2003, Timing and nature of Tertiary plutonism and extension in the Grouse Creek Mountains, Utah: International Geology Review, v. 45, p. 497–532, doi:10.2747/0020-6814.45.6.497.

Egger, A.E., Glen, J.M.G., and Ponce, D.A., 2010, The northwestern margin of the Basin and Range province: Part 2: Structural setting of a developing basin from seismic and potential field data: Tectonophysics, v. 488, p. 150–161, doi:10.1016/j.tecto.2009.05.029.

Ellis, B.S., and Wolff, J.A., 2012, Complex storage of rhyolite in the central Snake River plain: Journal of Volcanology and Geothermal Research, v. 211–212, p. 1–11, doi:10.1016/j.jvolgeores.2011.10.002.

Ellis, B.S., Barry, T., Branney, M.J., Wolff, J.A., Bindeman, I., Wilson, R., and Bonnichsen, B., 2010, Petrologic constraints on the development of a large volume, high temperature, silicic magma system: The Twin Falls eruptive center, central Snake River Plain: Lithos, v. 120, p. 475–489, doi:10.1016/j.lithos.2010.09.008.

Ellis, B.S., Wolff, J.A., Mark, D., and Bindeman, I., 2011, Widespread synchronous volcanism on the Snake River plain [abs.]: Mineralogical Magazine, v. 75, p. 806.

Ellis, B.S., Branney, M.J., Barry, T.L., Barfod, D., Bindeman, I., Wolff, J.A., and Bonnichsen, B., 2012, Geochemical correlation of three large-volume ignimbrites from the Yellowstone hotspot track, Idaho, USA: Bulletin of Volcanology, v. 74, p. 261–277, doi:10.1007/s00445-011-0510-z.

Ellis, B.S., Wolff, J.A., Boroughs, S., Mark, D.F., Starkel, W.A., and Bonnichsen, B., 2013, Rhyolitic volcanism of the central Snake River Plain: A review: Bulletin of Volcanology, v. 75, p. 745, doi:10.1007/s00445-013-0745-y.

Friedman, I., Lipman, P.W., Obradovich, J.W., Gleason, J.D., and Christiansen, R.L., 1974, Meteoric water in magmas: Science, v. 184, no. 4141, p. 1069–1072, doi:10.1126/science.184.4141.1069.

Gans, P.B., Mahood, G.A., and Schermer, E., 1989, Synextensional magmatism in the Basin and Range province: A case study from the eastern Great Basin: Geological Society of America Special Paper 233, 53 p., doi:10.1130/SPE233-p1.

Gottardi, R., Teyssier, C., Mulch, A., Vennemann, T.W., and Wells, M.L., 2011, Preservation of an extreme transient geotherm in the Raft River detachment shear zone: Geology, v. 39, p. 759–762, doi:10.1130/G31834.1.

Graham, D.W., Reid, M.R., Jordan, B.T., Grunder, A.L., Leeman, W.P., and Lupton, J.E., 2009, Mantle source provinces beneath the northwestern USA delimited by helium isotopes in young basalts: Journal of Volcanology and Geothermal Research, v. 188, p. 128–140, doi:10.1016/j.jvolgeores.2008.12.004.

Grunder, A.L., 1993, Two-stage contamination during crustal assimilation: Isotopic evidence from volcanic rocks in eastern Nevada: Contributions to Mineralogy and Petrology, v. 112, p. 219–229, doi:10.1007/BF00310456.

Hildreth, W., and Mahood, G., 1985, Correlation of ash-flow tuffs: Geological Society of America Bulletin, v. 96, p. 968–974, doi:10.1130/0016-7606(1985)96<968:COAT>2.0.CO;2.

Hildreth, W., Christiansen, R.L., and O'Neil, J.R., 1984, Catastrophic isotopic modification of rhyolitic magma at times of caldera subsidence, Yellowstone plateau volcanic field: Journal of Geophysical Research, v. 89, no. B10, p. 8339–8369, doi:10.1029/JB089iB10p08339.

Hildreth, W., Halliday, A.N., and Christiansen, R.L., 1991, Isotopic and chemical evidence concerning the genesis and contamination of basaltic and rhyolitic magma beneath the Yellowstone plateau volcanic field: Journal of Petrology, v. 32, p. 63–138, doi:10.1093/petrology/32.1.63.

Holk, G.C., and Taylor, H.P., 2007. $^{18}O/^{16}O$ evidence for contrasting hydrothermal regimes involving magmatic and meteoric-hydrothermal waters at the Valhalla Metamorphic Core Complex, British Columbia: Economic Geology, v. 102, p. 1063–1078, doi:10.2113/gsecongeo.102.6.1063.

Honjo, N., Bonnichsen, B., Leeman, W.P., and Stormer, J.C., Jr., 1992, High temperature rhyolites from the central and western Snake River Plain: Bulletin of Volcanology, v. 54, p. 220–237, doi:10.1007/BF00278390.

Hooper, P.R., Camp, V.E., Reidel, S.P., and Ross, M.E., 2007, The origin of the Columbia River flood basalt province: Plume versus nonplume models, *in* Foulger, G.R., and Jurdy, D.M., eds., Plates, plumes and planetary processes: Geological Society of America Special Paper 430, p. 635–668, doi:10.1130/2007.2430(30).

Kerrich, R., and Hyndman, D., 1986, Thermal and fluid regimes in the Bitterroot lobe–Sapphire block detachment zone Montana: Evidence from $^{18}O/^{16}O$ and geologic relations: Geological Society of America Bulletin, v. 97, p. 147–155, doi:10.1130/0016-7606(1986)97<147:TAFRIT> 2.0.CO;2.

Kita, N.T., Ushikubo, T., and Valley, J.W., 2009, High precision SIMS oxygen isotope analysis and the effect of sample topography: Chemical Geology, v. 264, p. 43–57, doi:10.1016/j.chemgeo.2009.02.012.

Konstantinou, A., 2013, Crustal evolution of the northeastern Basin and Range: Insights from the structural and magmatic history of the Albion–Raft River–Grouse Creek metamorphic core complex [Ph.D. thesis]: Stanford, California, Stanford University, 296 p.

Konstantinou, A., Strickland, A., and Miller, E.L., 2011, Nature and progression of magmatism in and around the Albion–Raft River–Grouse Creek metamorphic core complex: Geological Society of America Abstracts with Programs, v. 43, no. 4, p. 13.

Konstantinou, A., Strickland, A., Miller, E.L., and Wooden, J.W., 2012, Multi-stage Cenozoic extension of the Albion–Raft River–Grouse Creek metamorphic core complex: Geochronologic and stratigraphic constraints: Geosphere, v. 8, p. 1429–1466, doi:10.1130/GES00778.1.

Konstantinou, A., Strickland, A., Miller, E.L., Vervoort, J., Fisher, C.M., Wooden, J.P., and Valley, J., 2013, Magmatically induced diapiric rise of the Albion–Raft River–Grouse Creek metamorphic core complex, north-

eastern Basin and Range: Tectonics, v. 32, p. 1–20, doi: 10.1002/tect.20085 (in press).

Lackey, J.S., Valley, J.W., Chen, J.H., and Stockli, D.F., 2008, Dynamic magma systems, crustal recycling, and alteration in the central Sierra Nevada Batholith: The oxygen isotope record: Journal of Petrology, v. 49, p. 1397–1426, doi:10.1093/petrology/egn030.

Leeman, W.P., Menzies, M.A., Matty, D.J., and Embree, G.F., 1985, Strontium, neodymium and lead isotopic compositions of deep crustal xenoliths from the Snake River Plain: Evidence for Archean basement: Earth and Planetary Science Letters, v. 75, p. 354–368, doi: 10.1016/0012-821X(85)90179-7.

Leeman, W.P., Annen, C., and Dufek, J., 2008, Snake River Plain–Yellowstone silicic volcanism: Implications for magma genesis and magma fluxes: Geological Society of London Special Publication 304, p. 235–259, doi: 10.1144/SP304.12.

Lindsley, D.H., 1983, Pyroxene thermometry: American Mineralogist, v. 68, p. 477–493.

Ludwig, R.K., 2003, User's manual for Isoplot/Ex, Version 3.0, a geochronological toolkit for Microsoft Excel: Berkeley Geochronology Center Special Publication 4.

Mabey, D.R., and Wilson, C.W., 1973, Regional gravity and magnetic surveys in the Albion Mountains area of southern Idaho: U.S. Geological Survey Report Open-File Report 73-165, 12 p.

McCurry, M., and Rodgers, D.W., 2009, Mass transfer along the Yellowstone hotspot track I: Petrologic constraints on the volume of mantle-derived magma: Journal of Volcanology and Geothermal Research, v. 188, p. 86–98, doi:10.1016/j.jvolgeores.2009.04.001.

Miller, E.L., Dumitru, T.A., Brown, R.W., and Gans, P.B., 1999, Rapid Miocene slip on the Snake Range–Deep Creek range fault system, east-central Nevada: Geological Society of America Bulletin, v. 111, p. 886–905, doi: 10.1130/0016-7606(1999)111<0886:RMSOTS>2.3.CO;2.

Miyoshi, M., and 12 others, 2013, Lateral magma intrusion from a caldera-forming magma chamber: Constraints from geochronology and geochemistry of volcanic products from lateral cones around the Aso caldera, SW Japan: Chemical Geology, v. 352 p. 202–210, doi: 10.1016/j.chemgeo.2013.06.003.

Morgan, L.A., Doherty, D.A.J., and Leeman, W.P., 1984, Ignimbrites of the eastern Snake River plain: Evidence for major caldera-forming eruptions: Journal of Geophysical Research, v. 89, no. B10, p. 8665–8678, doi: 10.1029/JB089iB10p08665.

Nash, B.P., Perkins, M.E., Christensen, J.N., Lee, D.C., and Halliday, A.N., 2006, The Yellowstone hotspot in space and time: Nd and Hf isotopes in silicic magmas: Earth and Planetary Science Letters, v. 247, p. 143–156, doi: 10.1016/j.epsl.2006.04.030.

Parsons, T., Thompson, G.A., and Smith, R.P., 1998, More than one way to stretch: A tectonic model for extension along the plume track of the Yellowstone hotspot and adjacent Basin and Range Province: Tectonics, v. 17, p. 221–234, doi:10.1029/98TC00463.

Person, M., Mulch, A., Teyssier, C., and Gao, Y., 2007, Isotope transport and exchange within metamorphic core complexes: American Journal of Science, v. 307, p. 555–589, doi:10.2475/03.2007.01.

Pierce, K.L., and Morgan, L.A., 1992, The track of the Yellowstone hotspot: Volcanism, faulting, and uplift, *in* Link, P.K., et al., eds., Regional geology of eastern Idaho and western Wyoming: Geological Society of America Memoir 179, p. 1–53, doi:10.1130/MEM179-p1.

Pierce, K.L., and Morgan, L.A., 2009, Is the track of the Yellowstone hotspot driven by a deep mantle plume? Review of volcanism, faulting, and uplift in light of new data: Journal of Volcanology and Geothermal Research, v. 188, p. 1–25, doi:10.1016/j.jvolgeores.2009.07.009.

Pierce, K.L., Covington, H.R., Williams, P.L., and McIntyre, D.H., 1983, Geologic map of the Cotterel Mountains and the northern Raft River valley, Cassia County, Idaho: U.S. Geological Survey Miscellaneous Investigations Series Map I-1450, scale 1:48,000.

Rey, P.F., Teyssier, C., Kruckenberg, S.C., and Whitney, D.L., 2011, Viscous collision in channel explains double domes in metamorphic core complexes: Geology, v. 39, p. 387–390, doi:10.1130/G31587.1.

Rodgers, D.W., and McCurry, M., 2009, Mass transfer along the Yellowstone hotspot track II: Kinematic constraints on the volume of mantle-derived magma: Journal of Volcanology and Geothermal Research, v. 188, p. 99–107, doi:10.1016/j.jvolgeores.2009.05.014.

Rodgers, D.W., Hackett, W.R., and Ore, H.T., 1990, Extension of the Yellowstone Plateau, eastern Snake River Plain, and Owyhee Plateau: Geology, v. 18, p. 1138–1141, doi:10.1130/0091-7613(1990)018<1138:EOTYPE>2.3.CO;2.

Rodgers, D.W., Ore, H.T., Bobo, R., McQuarrie, N., and Zentner, N., 2002, Extension and subsidence of the eastern Snake River Plain, *in* Bonnichsen, B., et al., eds., Tectonic and magmatic evolution of the Snake River Plain volcanic province: Idaho Geology Survey Bulletin 30, p. 121–160.

Rollinson, H.R., 1993, Using geochemical data: Evaluation, presentation, interpretation (Longman Geochemistry Series): New York, Longman Scientific, 384 p.

Shervais, J.W., Branney, M.J., Geist, D., Hanan, B.B., Hughes, S.S., Prokopenko, A.A., and Williams, D.F., 2006, HOTSPOT: The Snake River Scientific Drilling Project–Tracking the Yellowstone hotspot through space and time: Scientific Drilling, v. 3, p. 56–57, doi: 10.2204/iodp.sd.3.14.2006.

Smith, J.F., Jr., 1982, Geologic map of the Strevell 15-minute quadrangle, Cassia County, Idaho: U.S. Geological Survey Miscellaneous Investigations Series Map I-1403, scale 1:62,500.

Stacey, J.S., and Kramers, J.D., 1975, Approximation of terrestrial lead isotope evolution by a two-stage model: Earth and Planetary Science Letters, v. 26, p. 207–221, doi:10.1016/0012-821X(75)90088-6.

Stewart, J.H., Moore, W.J., and Zietz, I., 1977, East-west patterns of Cenozoic igneous rocks, aeromagnetic anomalies, and mineral deposits: Nevada and Utah: Geological Society of America Bulletin, v. 88, p. 67–77, doi: 10.1130/0016-7606(1977)88<67:EPOCIR>2.0.CO;2.

Stockli, D.F., 1999, Regional timing and spatial distribution of Miocene extension in the northern Basin and Range Province [Ph.D. thesis]: Stanford, California, Stanford University, 478 p.

Strickland, A., Miller, E.L., and Wooden, J.L., 2011a, The timing of tertiary metamorphism and deformation in the Albion–Raft River–Grouse Creek metamorphic core complex, Utah and Idaho: Journal of Geology, v. 119, p. 185–206, doi:10.1086/658294.

Strickland, A., Miller, E.L., Wooden, J.L., Kozdon, R., and Valley, J.W., 2011b, Syn-extensional plutonism and peak metamorphism in the Albion–Raft River–Grouse Creek metamorphic core complex: American Journal of Science, v. 311, p. 261, doi:10.2475/04.2011.01.

Tanaka, T., and 18 others, 2000, JNdi-1: A neodymium isotopic reference in consistency with LaJolla neodymium: Chemical Geology, v. 168, p. 279–281, doi: 10.1016/S0009-2541(00)00198-4.

Taylor, H.P., Jr., 1986, Igneous rocks: II, Isotopic case studies of circum-Pacific magmatism: Reviews in Mineralogy and Geochemistry, v. 16, p. 273–317.

Thomson, B., Aftalion, M., McIntyre, R.M., and Rice, C., 1995, Geochronology and tectonic setting of silicic dike swarms related to silver mineralization in Candelaria, western Nevada: Economic Geology and the Bulletin of the Society of Economic Geologists, v. 90, p. 2182–2196, doi:10.2113/gsecongeo.90.8.2182.

Valley, J.W., 2003, Oxygen isotopes in zircon: Reviews in Mineralogy and Geochemistry, v. 53, p. 343–385, doi: 10.2113/0530343.

Valley, J.W., and Kita, N.T., 2009, In situ oxygen isotope geochemistry by ion microprobe, *in* Fayek, M., ed., Secondary ion mass spectrometry in the Earth sciences: Mineralogical Association of Canada Short Course 41, p. 19–63.

Vazquez, J.A., and Reid, M.R., 2002, Time scales of magma storage and differentiation of voluminous high-silica rhyolites at Yellowstone caldera, Wyoming: Contributions to Mineralogy and Petrology, v. 144, p. 274–285, doi:10.1007/s00410-002-0400-7.

Vervoort, J.D., Plank, T., and Prytulak, J., 2011, The Hf-Nd isotopic composition of marine sediments: Geochimica et Cosmochimica Acta, v. 75, p. 5903–5926, doi: 10.1016/j.gca.2011.07.046.

Watts, K.E., Leeman, W.P., Bindeman, I.N., and Larson, P.B., 2010, Supereruptions of the Snake River plain: Two-stage derivation of low-delta $^{18}O$ rhyolites from normal-delta $^{18}O$ crust as constrained by Archean xenoliths: Geology, v. 38, p. 503–506, doi:10.1130/G30735.1.

Watts, K.E., Bindeman, I.N., and Schmitt, A.K., 2011, Large-volume rhyolite genesis in caldera complexes of the Snake River Plain: Insights from the Kilgore tuff of the Heise volcanic field, Idaho, with comparison to Yellowstone and Bruneau-Jarbidge rhyolites: Journal of Petrology, v. 52, p. 857–890, doi:10.1093/petrology/egr005.

Weiss, D., Kieffer, B., Maerschalk, C., Pretorius, W., and Barling, J., 2005, High-precision Pb-Sr-Nd-Hf isotopic characterization of USGS BHVO-1 and BHVO-2 reference materials: Geochemistry, Geophysics, Geosystems, v. 6, doi:10.1029/2004GC000852.

Wells, M.L., 2009, Geologic map of the Kelton Pass quadrangle, Box Elder County, Utah, and Cassia County, Idaho: Utah Geological Survey Miscellaneous Publication 09-3, scale 1:24,000.

Wells, M.L., Snee, L.W., and Blythe, A.E., 2000, Dating of major normal fault systems using thermochronology: An example from the Raft River detachment, Basin and Range, western United States: Journal of Geophysical Research, v. 105, no. B7, p. 16303–16327, doi:10.1029/2000JB900094.

Williams, P.L., Pierce, K.L., McIntyre, D.H., and Schmidt, P.W., 1974, Preliminary geologic map of the southern Raft River area, Cassia County, Idaho: U.S. Geological Survey Open-File Report 74-1126, scale = 1:24,000.

Williams, P.L., Covington, H.R., and Pierce, K.L., 1982, Cenozoic stratigraphy and tectonic evolution of the Raft River Basin, Idaho: Idaho Bureau of Mines and Geology Bulletin 26, p. 491–504.